Design and Fabrication of Meso-scale Flexural Testing Apparatus for Evaluating Aligned CNT
Composite Flexures

by

Robert M. Panas

Submitted to the Department of Mechanical Engineering
in Partial Fulfillment of the Requirements for the Degree of
Bachelor of Science in Mechanical Engineering

at the

Massachusetts Institute of Technology

May 2007

[June 2007]

Signature of Author...
Department of Mechanical Engineering
May 11, 2007

Certified by...
Martin L. Culpepper
Rockwell International Associate Professor of Mechanical Engineering
Thesis Supervisor

Accepted by..
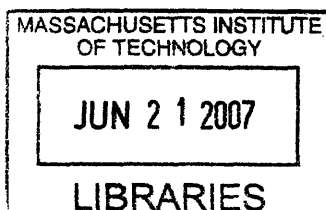John Lienhard V
Professor of Mechanical Engineering
Chairman, Undergraduate Thesis Committee

Design and Fabrication of Meso-scale Flexural Testing Apparatus for Evaluating Aligned CNT
Composite Flexures

by

Robert M. Panas

Submitted to the Department of Mechanical Engineering
on May 11, 2007 in Partial Fulfillment of the
Requirements for the Degree of Bachelor of Science in
Mechanical Engineering

ABSTRACT

The objective of this research is to explore the possibility of using aligned Carbon Nanotube (CNT) based composites in flexures by measuring the kinematics of a composite flexure. The first phase of the research, described in this thesis, is to design, fabricate and assemble a testing apparatus optimized for evaluating aligned CNT based composites. Using existing literature on composites and present limitations on their growth, functional requirements are set down for the testing apparatus. Several designs are qualitatively evaluated, leading to a near optimal design form. This chosen design is modeled as a spring-mass system, and the exact geometry needed to satisfy the functional requirements is determined. The design of the full apparatus is expanded to contain the necessary probes and actuators. The testing apparatus is fabricated using CNC machining, and assembled in a controlled environment to reduce thermal and mechanical error during operation. The system is calibrated and its resolution is found to be 0.021 N over a range of 28.5 N applied force and 1.5 µm over a range of 816 µm applied displacement. Several non-linearities are noted and corrected mathematically.

Thesis Supervisor: Martin L. Culpepper
Title: Rockwell International Associate Professor of Mechanical Engineering

ACKNOWLEDGEMENTS

I would like to thank Prof. Martin Culpepper for the fantastic academic opportunities he has made available to me throughout my undergraduate time at MIT. I have learned a great deal of engineering and research from him, and have every intention of learning much more through graduate school.

I would also like to thank my family and fiancée for their unwavering support of my academic goals despite my own doubt at times.

Table of Contents

List of Figures

List of Tables

Chapter 1

Introduction

The objective of this research is to explore the possibility of using aligned Carbon Nanotube (CNT) based composites as flexures in compliant mechanisms by determining the kinematics of a composite flexure. This will make it possible to evaluate the composite by comparison with existing materials. Compliant mechanisms are devices which contain mechanical components whose kinematics are dominated by material strain [1]. CNT-based flexures are important because they may have much greater yield strength and yield strain than commonly used flexure materials. The result of this material based improvement would be to increase the range over which compliant mechanisms can operate for a given size, or allow for miniaturization of the devices while maintaining a given operating range. Smaller flexural devices could be used in translation stages integrated into devices with strict size requirements, such as SEMs and TEMs, for rapid and precise movement of the sample.

This research is separated into two general phases, first being the design and fabrication of a testing apparatus in which to measure the effectiveness of the flexures, the second being the fabrication and testing of the CNT composite flexures themselves. The second phase of the research is being worked on at the time of writing, limiting the scope of this thesis to the first phase; design and fabrication of the testing apparatus.

1.1 Background on Compliant Mechanisms

1.1.1 Components

It is first important to be aware of the strengths and shortcomings of compliant mechanisms in order to understand the possible benefits of CNT composite flexures. As briefly mentioned before, compliant mechanisms are devices which utilize material strain to produce motion in a predictable manner. The strain-based deformation is limited to small sub-sections of

the device known as the flexures. Compliant mechanisms will contain at least some of these components;

- Flexures that are capable of the desired deformation.

- Rigid members which will undergo the translation motions that are allowed by the flexures.

- Support structure onto which the non-mobile ends of the flexures are anchored.

- A method of actuation to produce the stress required in strain-based deformation.

- A system of metrology to determine the state of the device.

These components are illustrated in the simplified model of a probe-based nano-manufacturing compliant mechanism shown in Figure 1.1 below, where a capacitance actuator (4) electrostatically repels the rigid member (2), driving it into a surface so as to score the surface. Flexures (1) attached to both the rigid member and support structure (3) act as linear bearings and a returning force, so the actuation need only be repulsive. A small sensor (5) reads back the location of the rigid member, thereby enabling for closed-loop control of the system.
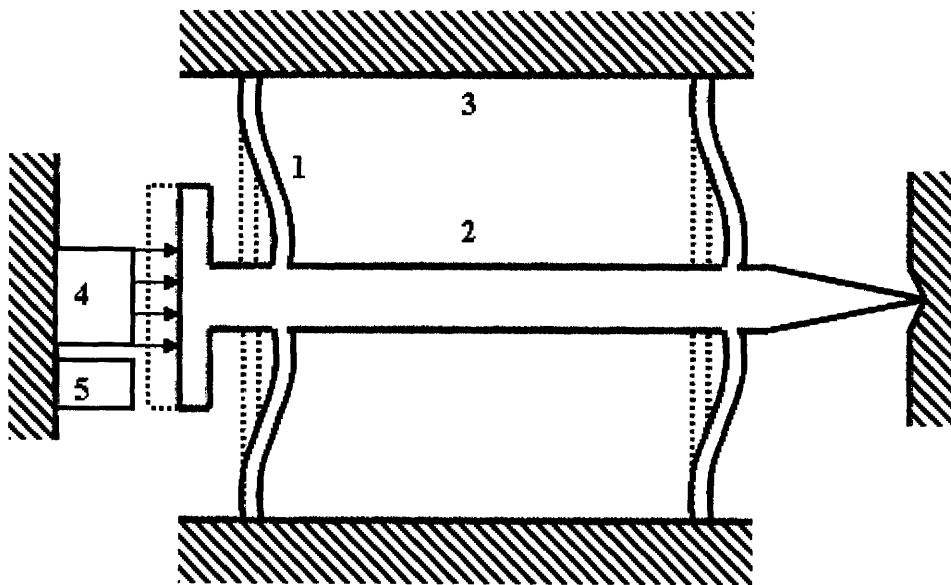
Figure 1.1: Probe-based manufacturing as example of compliant mechanism.

The flexures in a compliant mechanism are generally shaped to be as flexible as possible in a particular direction, resulting in ribbon or even accordion-like geometries. The flexures are made as stiff as possible in the other directions in order to restrict some degrees of freedom.

The motion produced by the deformation of flexures is generally applied to some rigid member at the end of the flexure, thus approximating classically non-compliant devices with

discrete bearings and moving components. This rigid member may be the 'non-mobile support' for another set of flexures, or may carry some device on it.

The support structure onto which the flexures are anchored provides the necessary resistive forces on the flexures, and thus translational rigid members, to keep the device stationary despite the deformation inducing forces on it. In the case of small-scale compliant mechanisms, the support structure can be a large fraction of the total volume of the machine, so as to provide a multi-scale interface. However, this mis-match in scale reduces the benefits of the miniaturization effort.

The method of actuation is usually integrated into the mechanism, as in the case of micro-electro-mechanical systems (MEMS) in which an electrostatic actuator is fabricated as part of one of the rigid members, or as a linear motor of some sort, anchored to the support structure. Not all compliant mechanisms require integrated actuation, as they may be part of a human interface or some other system, where the actuation is provided by a separate component.

A system of metrology- measurement- is often part of small-scale compliant mechanisms, and used to provide information that is necessary to determine the exact location, or the output of the device. This is common in smaller-scale devices, as their state may not be visible. For larger scale devices such as a human interface described above or non-precision mechanisms, there is likely no need for any integrated metrology system.

1.1.2 Benefits

Using permutations of the common components described above, compliant mechanisms may be designed to exhibit many strengths, including 1) deterministic output, 2) specified stiffness in all three axes, 3) monolithic fabrication, 4) large cyclic lifetime and highly repeatable response to input, and 5) low energy losses to friction.

The flexures which produce translation or rotation in compliant mechanisms rely on elastic deformation, which is modeled as a linear spring with a spring constant that is dependent on the material properties and geometry of the flexure. This results in a linear one-to-one function between input (force) and output (displacement), which underlies the deterministic nature of the compliant mechanism. The normal backlash and hysteresis expected in rigid, discrete mechanisms does not occur in flexures. This non-deterministic movement is the result of the gaps required for motion between the separate components, a situation which is

circumvented by the use of material deformation rather than gaps as bearings in compliant mechanisms.

The stiffness of a flexure is dependent on both its material properties and geometry. Material properties like Young's Modulus, yield stress, and to a lesser degree the Poisson ratio factor into the relation between stress and strain on a microscopic scale within the flexure. They also serve to set limits on the elastic range. The geometry of the flexure determines the relation between the microscopic strain and total deformation. The result in many cases is an analytical expression that describes the deformation of the flexure as a function of the applied force in any direction this enables the calculation of an effective vector stiffness to characterize the flexure.

For the example shown in Figure 1.2 below, the vector stiffness is found through a straightforward application of the stress-strain relation (in the axial direction), and double integration of the Euler-Bernoulli bending expression (in the two orthogonal-to-axial directions).
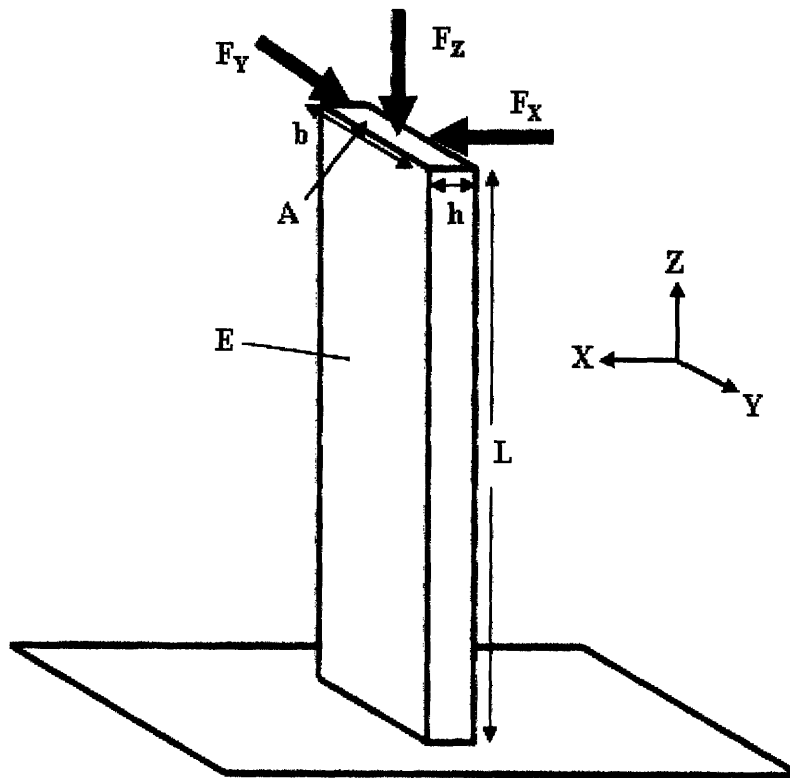

Figure 1.2: A compliant parallel-guiding mechanism.

The axial stiffness is calculated by considering the flexure to be a solid bar of material subjected to a normal load, F_z, on its tip, resulting in displacement z at the location of the force application, in the direction of F_z. This is shown by Eq. 1.1 below, where E is the Young's

Modulus of the material, A is the transverse cross-section of the block and L is the axial length of the block.

$$\frac{F_z}{A} = E\frac{z}{L}$$ (1.1)

Using the linearity of the expression, the axial stiffness k_z, may be expressed as shown in Eq. 1.2.

$$\frac{F_z}{z} = k_z = \frac{AE}{L}$$ (1.2)

To calculate the two transverse stiffnesses, the beam is assumed to be isotropic and to have a neutral strain plane along its axis. It is also assumed to be a slender member, with length much greater than base or height. The deformation may then be described by the Euler-Bernoulli beam bending expression as in Eq. 1.3,

$$\frac{\partial^2 x}{\partial z^2} = \frac{M(z)}{EI},$$ (1.3)

where z is axial distance down the beam, x is displacement orthogonal to the axis, $M(z)$ is the moment as a function of axial location, and I is the bending moment of the beam. For a rectangular beam similar to the one shown in Fig. 1.2, the bending moments in the x and y directions, I_x and I_y respectively, are expressed as shown in Eq. 1.4 below. The width, b, and thickness, h, are aligned as shown in Fig. 1.2.

$$I_x = \frac{bh^3}{12}$$
$$I_y = \frac{hb^3}{12},$$ (1.4)

Using these two bending moments (Eq. 1.4), and the Euler-Bernoulli bending equation (Eq. 1.3), an equation linearly relating force to displacement may be found for the flexure in Fig. 1.2. If this is instead written as a stiffness, the off-axis spring constants may be written as shown in Eq. 1.5 below.

$$k_x = \frac{3Ebh^3}{12L^3}$$
$$k_y = \frac{3Ehb^3}{12L^3},$$ (1.5)

Using the three orthogonal stiffnesses determined above in Eq. 1.2 and 1.5, the vector stiffnesses of the flexure may be analytically expressed, linking the beam geometry (L, b, h) to the flexure's three dimensional kinematics. This is usually done in such a way that the stiffness

of the flexure in the direction of its intended movement is upwards of orders of magnitude lower than the stiffnesses in the other directions. Given this, the beam may be treated as a compliant 'bearing' in one direction, and rigid 'restraint' in the other directions. This mimics the limited degrees of freedom found in the bearings of rigid discrete mechanisms, geometrically solving the problem presented by the isotropic nature of the flexural material.

Compliant mechanisms produce movement from material elasticity rather than the motion of discrete parts, so they may be fabricated as single monolithic components. The support structure, flexures and rigid members may all part of the same piece. Rather than assembling separate parts into a bearing, compliant mechanisms make it possible for the entire structure to be cut out from a single block. The benefit of this method lies in the absence of a need for assembly. Since they are cut in place, the flexures are under no strain initially. Also, whereas in a regular assembly, a part may be over-constrained by guiding it with too many linear bearings, in a compliant mechanism this problem does not occur. With each flexure machined into place, the flexures are all the exact length, thereby placing no theoretical limits on the number of flexures that may be used in parallel as bearings. Given that all of the components are permanently fused together, there is no need for the complex and occasionally non-linear models required to predict the exact response of screwed or bolted joints to stresses. Instead, the whole system may be analyzed simultaneously with finite element modeling (FEM).

Flexures are operated in the elastic region of the material; in this region standard material theory states that the deformation induced by the applied force is not permanent. This means that the flexure is theoretically and practically unaltered by use, as compared to the wear and friction that accumulates in mechanisms with discrete components. With low accumulated damage, the flexures demonstrate high repeatability. Additionally, the low cyclic damage results in very long cyclic lifetimes. Finally, the repeatability means that the loading and unloading curves show nearly the same shape and thus the areas under them are nearly equal. This implies that the energy absorbed by the flexure in loading is almost exactly the same as the energy lost from the flexure in unloading, leaving almost no room for energy dissipation. This theoretical argument is reinforced by the common observation of extremely low damping coefficients (lost energy) in flexures subjected to dynamics.

1.1.3 Disadvantages

The drawbacks of compliant mechanisms result from the same principles in which their strengths lie; 1) the scale of flexures must be much greater than their intended range of motion, 2) the degrees of restraint are not absolute, and 3) the mechanisms generally are confined to two dimensions.

The flexures in a compliant mechanism must normally be between roughly one and two orders of magnitude larger in scale than the range of movement in order to produce the needed range of deformation. This produces bulky structures that may easily become multi-scale, inheriting all of the problems associated with such structures, such as energy, momentum, or even electrical flows from the larger component. While these flows are dismissed as inconsequential to the larger scale components, they can easily damage the smaller-scale components. The design of multi-scale systems is significantly more complex than the design of single scale systems due to the need to account for many (normally ignored) higher-order effects.

The vector stiffnesses of a flexure may be adjusted to produce order of magnitude differences between the directional components. However, this may be compared to discrete rigid component mechanisms, where the scale of the force to drive an object along its bearing-guided degree of freedom is friction based while the scale of the force to drive an object along a degree of restraint is material-elasticity based (because of rigid limits). This is in contrast to flexures where both are elasticity based. The inherent difference between the two ratios is such that while proper design can minimize parasitic motion in compliant mechanisms, the parasitic motion must still be accounted for in the kinematics. This is especially relevant in precision compliant systems design.

Two or 2½ dimension machining methods are generally the only options to produce the arbitrary shapes and interior cuts on a block of material required to produce a detailed monolithic compliant machine. For example, meso- to macro-scale compliant mechanisms are commonly made with laser-cutting or water-jet cutting. Micro-scale compliant mechanisms are generally made through photolithography. This restricts flexural designs to largely be planar layouts of components, restricting the complexity of the devices somewhat.

Compliant mechanisms have mainly found use in precision devices because of their particular combination of strengths and drawbacks. These are used in research tools such as atomic force microscopes or in commercial wafer fabrication machines, both of which must be

repeatable and accurate. The high cost of these devices (AFM, wafer machine) mean that the extra complexity and size required by compliant mechanisms are not a significant drawback. A growing field for compliant mechanism design is Micro-Electro-Mechanical-Systems (MEMS). The most effective bearings for MEMS have been found to be flexures, and the monolithic fabrication requirement fits well with the only method of machining on that level- photolithography. The most common use for MEMS is sensing, such as accelerometers and pressure gauges.

1.2 Background on Carbon Nanotubes

1.2.1 Individual CNT Structure

Carbon Nanotubes comprise the other half of the technology on which this thesis is focused. These structures may be envisioned as atomic-scale graphene sheets wrapped into a cylinder to form straw-like geometries, often orders of magnitude longer than they are wide.

Pure carbon can exist in multiple different forms, known as allotropes. The allotrope of greatest interest to carbon nanotube research is graphene, for the small-scale molecular structure of graphene is generally understood to be the same as that composing nanotubes. Graphene is a flat sheet of single atom thickness, composed of carbon atoms that are each bonded to three other atoms with the sp^2 hybridized bonds of length 1.42 Å at angles of 120° to each other. This gives rise to an array of hexagonal outlines formed by the carbon-carbon bonds. When the sheets are stacked, van-der-Waals forces act to maintain an equilibrium distance of 3.4 Å between sheets, which is accepted as the effective 'thickness' of the sheet [2].

Carbon Nanotubes were first discovered by S. Iijima in 1991 [3], and have been the objects of intense study since that time, particularly because of their characteristics of self-assembly , atomic scale perfection and great strength, with Young's Modulus of roughly 1.2 TPa and yield stress of roughly 100 GPa [2]. CNTs bridge the gap from micro to nano-engineering, as they are only dozens to a few hundred atoms wide but have been observed to be upwards of centimeters long [4]. Owing to the difficulty in effectively utilizing their incredible nano-scale properties on meso- or larger scale devices, little success has been made in incorporating CNTs into mechanical devices,. In contrast, composites of homogenously distributed CNTs in epoxy have received a great deal of attention, but the tendency of CNTs to clump at high volume

fractions has limited the strength gains to be found in making these composites [5]. Aligned CNT arrays have received much less attention, owing to the inherent difficulty in producing a truly aligned system of nano-scale structures, as well as the anisotropy of the material that is produced. However, the aligned nature of the tubes may enable greater utilization of their nano-scale properties if they are fabricated correctly.

Carbon Nanotubes may be viewed as rolled graphene sheets with opposite edges fused together to form a single-walled tube of a uniform diameter that may vary from about 0.4 nm to 50 nm [6,7]. The axial dimensions of the nanotube span from the microscopic to the macroscopic- with a diameter of only a few hundred atoms, the length of a single-walled tube has been measured up to about 4 centimeters, upwards of 10^7 times the diameter [4].
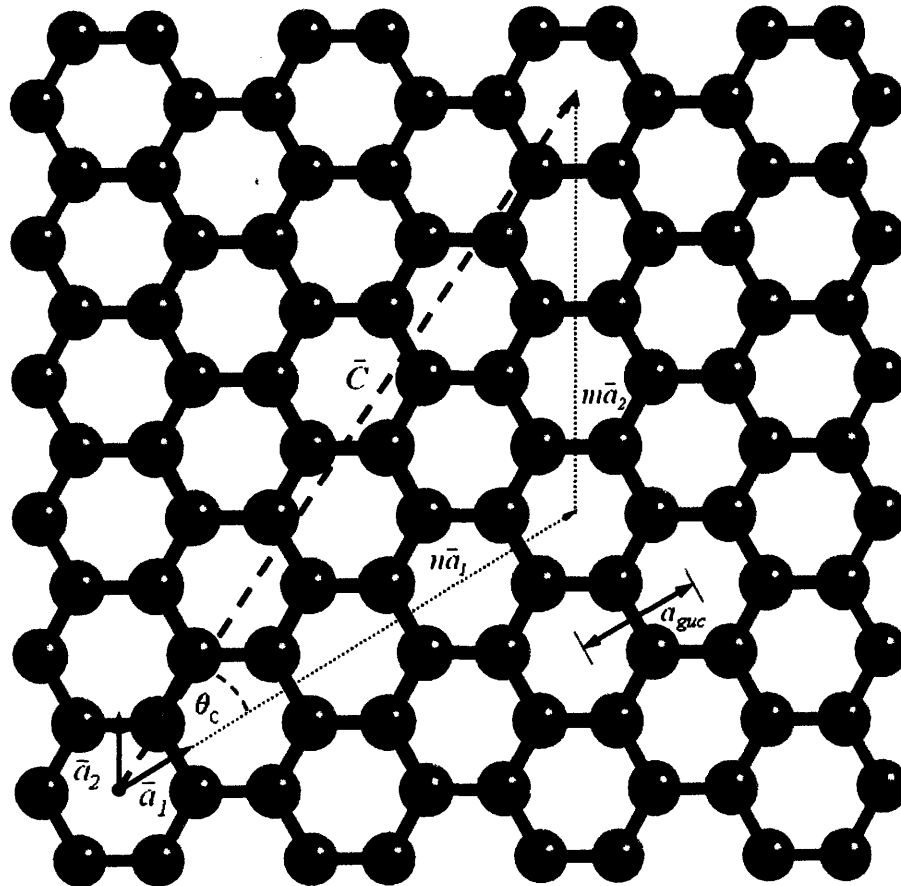

Figure 1.3: Diagram of the method for determining chirality of a nanotube.[1]

CNTs also possess the characteristic of chirality, which is a measure of the helicity of the graphene sheet walls of the nanotube. Chirality may most easily be envisioned by imagining that the wall of the tube is cut through a particular atom. The tube is then unrolled with the same length and a width equal to the circumference of the tube. Starting at the particular cleaved atom, a wrapping vector C is drawn back to the other part of this atom at the opposite edge of the sheet. This vector describes the both the wrapping angle and circumference since it perfectly circumscribes the tube. The vector C is specified by two values (n,m) in the equation ($C = na_1+ma_2$) where a_1 and a_2 are unit vectors along the two main axes of a graphene sheet. These axes are shown in Fig 1.3 above, and correspond to two of the six primary directions inherently marked out in a hexagonal lattice by the faces of each hexagon. In the specific case where $m = 0$, the wrapping angle is $0°$ and the chirality is described as 'zigzag', and when $n = m$, the wrapping angle is $30°$ and the chirality is described as 'armchair'. All other tubes fall between these two extremes, and are simply described as 'chiral' with a given (n,m) pair.

The chirality of a Carbon Nanotube has a large effect on its electrical properties. Tubes whose chirality is such that $n - m = 3*l$ (where l is any integer) show the electrical properties of a metallic conductor, while those which do not satisfy that mathematical condition show the electrical properties of a semiconductor [7]. However, the chirality of a nanotube does not appear to significantly affect its mechanical properties [8,9].

1.2.2 CNT Composites

A great deal of focus has been placed on the use of CNTs as reinforcing filaments in an epoxy matrix in the same way that carbon fiber is used (on a much larger scale) to make resilient composites. The typical fabrication process involves mixing small tubes (of length far less than 1 mm) into a liquid epoxy, utilizing both chemical and mechanical means to homogenously distribute the tubes throughout. These composites have shown both stiffness and yield stress gains over the epoxy material itself; however the boosts in properties have been limited by the ability to evenly distribute CNTs through the composite. Past a certain volume fraction of about 5%, it becomes prohibitively challenging to prevent the clumping of CNTs, thereby ruining the composite properties [5].

Alternately, some more recent efforts have involved the formation of aligned-CNT composites [10]. In these cases, CNTs are grown in particular formations that are based off of

catalyst placement. The formations are then wetted with an epoxy and dried to form a composite that derives its structure from the initial geometry of the CNTs. In these cases, the problem of clumping is not an issue, for the CNTs run the whole length (or height) of the material. In doing so, the CNTs are twisted and wrapped up inextricably with one another, thereby making a strong mechanical connection between themselves and with the matrix. The essential difference between the distributed and aligned states is the dimensions of the CNTs relative to the dimensions of the composite.

1.3 Importance

The benefits of aligned-CNT composites lie in their theoretical ability to utilize the extraordinary strength and stiffness of nanotubes on a much larger scale, with the result of large gains in the yield stress. For flexures, this gain translates to an increase in elastic range, and an anisotropic boost in stiffness. This anisotropy may be utilized to boost the ratio between restraint and bearing stiffness. Compliant mechanisms that utilize aligned-CNT composites would then be able to achieve equivalent translational ranges with smaller structures, as compared to compliant mechanisms made of presently used materials. This would aid in the miniaturization of components which cuts costs and increases the possible applications for the devices.

Chapter 2

Initial Design Process

2.1 Initial Design Requirements

The design of the testing apparatus begins with the overall goal that the apparatus is intended to achieve- to apply a transverse deflection on a composite CNT flexure, measuring both force and displacement during the deflection. The composite flexure will be made of aligned CNTs in an epoxy matrix.

Several requirements were determined for the testing apparatus. Primarily, these requirements were derived from the limits on the available CNTs. In order to produce an aligned-CNT flexure, a nanotube forest of at least the flexure length was required. The tallest CNT forests available for use were 3mm, which were obtained from Dr. Anastasios John Hart working with Prof. Alexander Slocum at the Precision Engineering Research Group (MIT). Using this characteristic height, back of the envelope calculations were done to determine the force and displacement range of needed for the testing apparatus. In order to produce flexure-like behavior (deformation mechanics dominated by normal stress- tension and compression- rather than shear stress) the thickness of the composite structure needed to be on the order of 0.3mm. The width was assumed to be roughly that of the sample, slightly over 5 mm.

The material of the flexure was calculated assuming it to be a common polymer, since it was assumed that the composite would be made from CNTs interspersed throughout an epoxy polymer. As mentioned earlier, the low density of CNTs means that the material properties of the composite are generally close (order of magnitude) to the properties of the polymer matrix alone. This produced a rough estimate of the force range to be on the scale of 10 N and the displacement range to be on the scale of 500 μm.
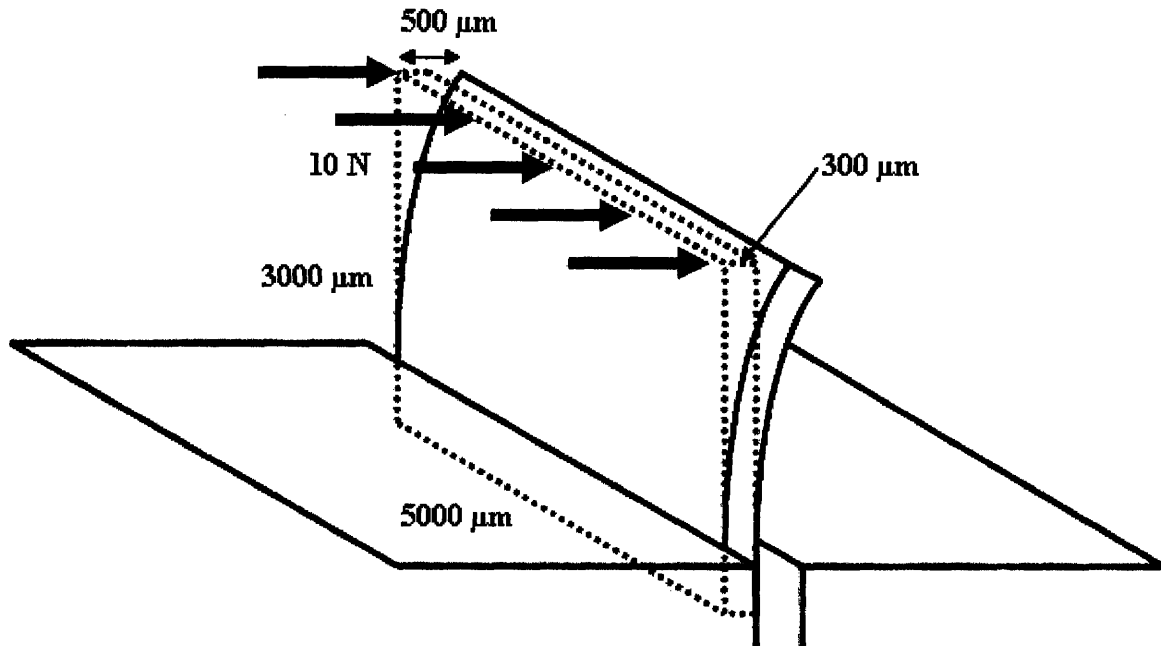
Figure 2.1: Initial outline of flexure testing geometry.

The apparatus needed to be capable of being adapted to working with flexures, requiring an anchor system at one end of the flexure and a method of applying force along a line parallel to the anchor. These requirements are demonstrated in the initial model shown in Figure 2.1 above, and listed in Table 2.1 below.

Table 2.1: Functional requirements

Requirement	Value
Range of Deflection	$\approx 500 \ \mu m$
Range of Force	$\approx 10 \ N$

2.2 Evaluation of Existing Designs

Several existing machines were considered for use, including available macro-scale static material testing machines such as the 'Allround-Line©' produced by Zwick, and significantly smaller scale machines such as the 'TriboIndenter©' produced by Hysitron, before it was decided that a custom testing device would be required.

25
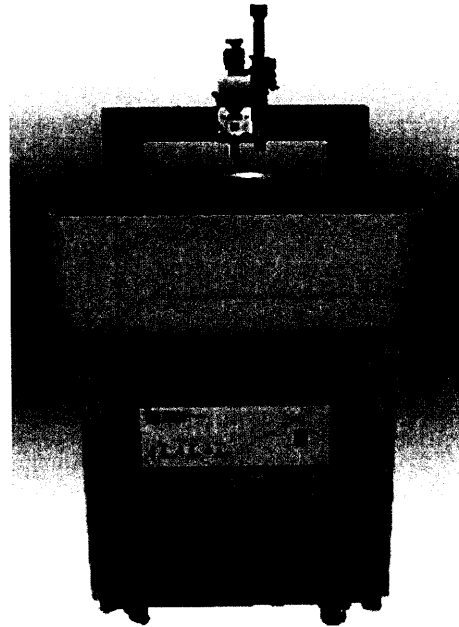
(a)   (b)

Figure 2.2: Zwick Allround-Line© testing machine[2] (a), and Hysitron TriboIndenter©[3] (b).

The Zwick testing machine, shown in Figure 2.2(a) above is capable of applying a force on the anchored material up to 250 kN, and measuring the displacement over a range of roughly 60 cm with a resolution of 2 μm [11]. While this covers the required ranges for the flexural testing apparatus, the orders of magnitude by which it overshoots the required range mean that the entire experiment would occur at the scale of the machine's minimum resolution, hindering efforts to gather accurate results. The machine operates on the macro-scale, so trying to use it to cause micro-scale deflections on meso-scale flexures is simply pushing below the useful operating range.

The second available machine considered was the Hysitron 'TriboIndenter©', shown in Figure 2.2(b) above. This testing machine has an optional probe tip that can apply a set force and measure displacement. This setting, called the '3D OmniProbe©' is designed to indent and scratch the surface of a material, which enables for detailed measurements of the micro-scale surface hardness. The lateral force range for the device is up to 5 N with a resolution of 50 μN,

---

[2] Figure 2.2(a) reproduced with permission from < http://www.zwick.com/upload/_machines_and_devices_EN/66 _935/Z100-metal.jpg>. Copyright 2004 by Zwick GmbH & Co. KG, Ulm, Germany.

[3] Figure 2.2(b) reproduced with permission from <http://www.hysitron.com/ImagesNew/product_triboindenter.jpg>. Copyright 2007 by Hysitron, Inc. USA.

26

and the lateral displacement range is up to 15 cm, with a resolution of 0.5 µm [12]. These values matched much more closely to the testing apparatus requirements, however they fall below with regards to the force range, meaning that the flexures would have to be made significantly thinner (so as to operate well beneath the 5 N ceiling). While this would not have been impossible, the second set of requirements dealing with anchoring and force application disqualified this machine for use. The Hysitron machine allowed no straightforward way in which the sharp, scratching tip of the probe could be altered to apply an evenly distributed force over a horizontal line another the flexures edge. In contrast, components could be attached to the compression plates of the Zwick testing machine to both anchor the flexure and apply a force evenly over the far tip of the composite flexure.

In the absence of an available machine to use for testing, it was determined that a device would need to be designed and built specifically for this purpose. Designing and fabricating a device uniquely for this task would mean that the force and displacement ranges of the testing apparatus could be exactly matched to the requirements posed by the flexure material and geometry. Additionally, the anchoring structure and the force application structure could both be integrated into the device, thereby reducing the complexity and hence associated error of these interfaces.

2.3 Initial Design Concepts

Several design concepts were evaluated for their apparent effectiveness in meeting the initial design requirements outlined in section 2.1. The designs were also evaluated for robustness, possible sources of error and simplicity.

2.3.1 Design 1: Pulling via Wire

The first design was an attempt to solve the most obvious problem of applying a constant force on the flexure tip without restraining the parasitic vertical motion that is caused by deforming the flexure. This design is shown in Figure 2.3.
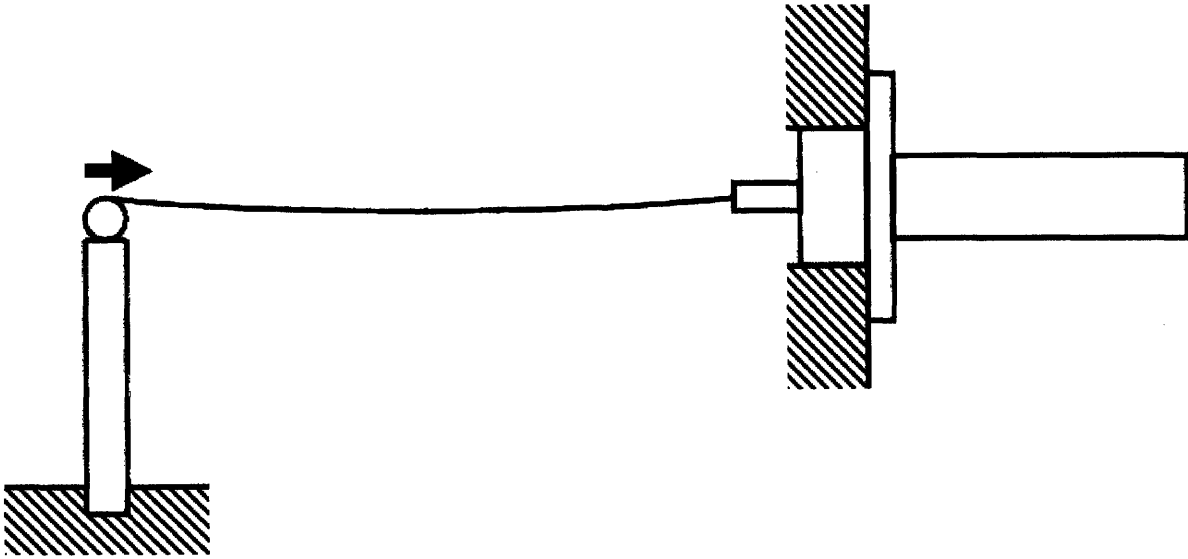
Figure 2.3: Depiction of design 1.

A clip or bar would be attached to the top of the flexure, and a wire run from the bar horizontally to a displace-able anchor, such as a micrometer. The length of the wire would minimize the vertical component of the applied force even accounting for the previously mentioned parasitic vertical motion of the composite flexure. While the wire concept effectively solved the issue of constraints and degrees of freedom on the flexure, the practical instantiation of this was problematic. The anchoring bar on the top of the flexure would need to be glued onto the top, as any method involving screws would require such a large bar that it would likely crush the flexure under its weight. Additionally, the design showed for no straightforward method for measuring the amount of force applied by the wire. Finally, the wire, anchoring system and bar to flexure interface would have to be stiff enough that its stretched was confined to the sub-micron range, otherwise the stiffness of the system in series with the flexural stiffness would cause significant error. The glue interface between the bar and flexure could easily have a large elasticity, and the anchoring points for the wire would suffer from creep. Finally, the large length of the wire would increase its already significant compliance. The benefits of this design were condensed and incorporated into the second design, described below.

2.3.2 Design 2: Pulling via Flexure

The second design iteration focused on reducing inherent error in measurement through accounting for the various stiffnesses of the testing apparatus. The system would still be actuated by a micrometer, as shown in Figure 2.4.
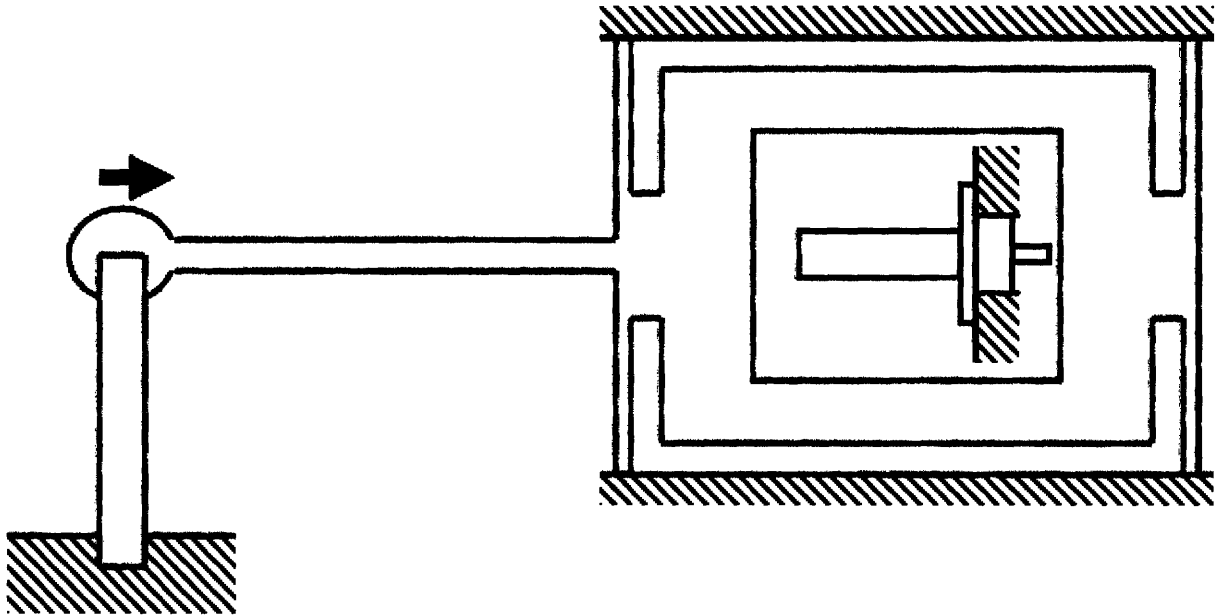

Figure 2.4: Depiction of design 2.

The change involved replacing several of the components with flexures, whose deformation could be predicted. The wire was replaced with a solid beam, guided by a four-bar shuttle to act as a linear bearing for the bar. .

The large length of the bar would allow it to freely flex vertically, retaining the horizontal degree of constraint and vertical degree of freedom at the flexure tip. The compressive or tensile stiffness (horizontal in the figure above) would be significantly higher than the off-axis stiffness, so that the bar could be treated as vertical bearing. A more complex, clamping interface at the flexure tip could now be supported by the solid beam, removing the glue interface, and the elasticity issues associated with it. However, in supporting the clamping interface, the beam added a rotational degree of constraint, which was undesired. This could be accounted for when producing a constitutive relation relating the composite flexure material properties to its force and deformation, but it was not ideal. The top clamping could easily damage the flexure or pinch it to create another joint. Finally, the design again did not incorporate a direct way to

measure force. Based off of these problems, the design was again reworked with the beneficial features retained, to produce the next iteration.

2.3.3 Design 3: Pushing via Flexure

The third design iteration replaced the pulling concept for deforming the composite flexure with a pushing concept, which removed the need for a clamp at the end of the flexure, as shown in Figure 2.5.
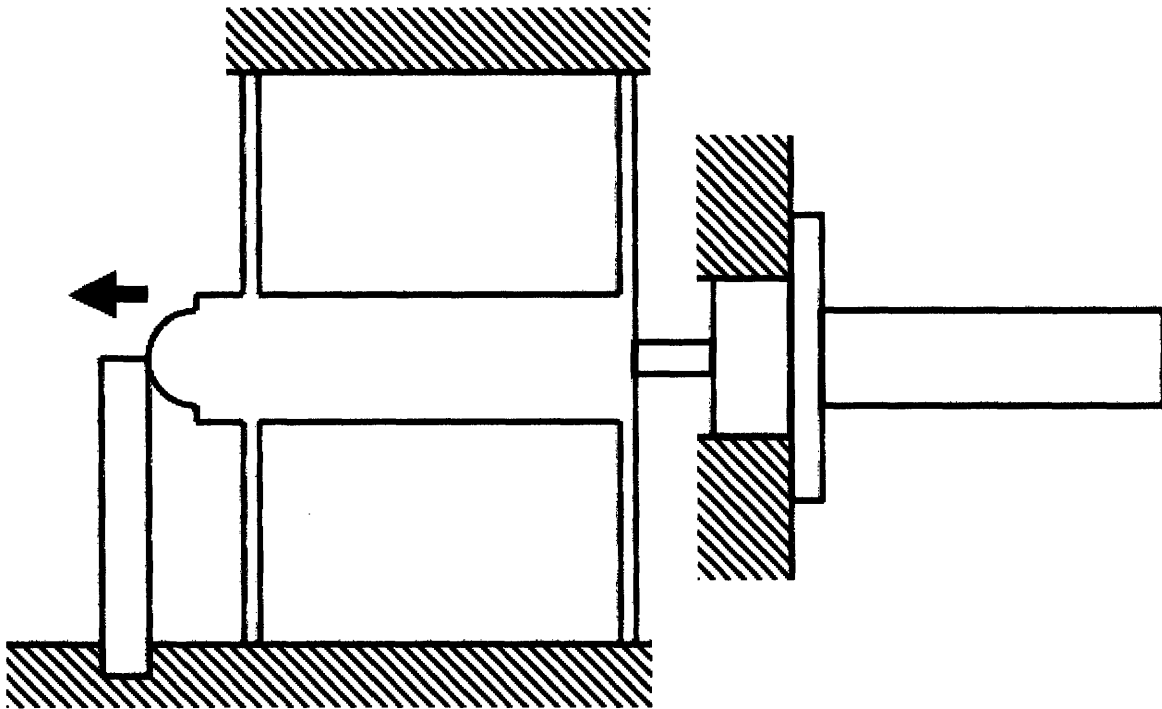
Figure 2.5: Depiction of design 3.

The tip of the composite flexure would no longer be rotationally constrained so it could be treated once again as the simple model presented in Section 1.1. The main bar which contacted the flexure was still linked to a flexure-based 4-bar linear bearing, and would be actuated by a micrometer.

With no clamping or gluing, the flexure would be free to slide slightly along the pushing surface as the flexure deformed. Additionally, the stiffnesses of the testing apparatus would no longer interfere with the measurement of the composite flexure's displacement, as none of equivalent scale were placed in series (or parallel) with the flexure. This design effectively solved the problem of force application and displacement measurement, however as with all the previous designs, this design also did not have any method for force measurement.

30

2.3.4 Design 4: Pushing via Flexure and Force Measurement

To measure the force applied to the flexure, a small flexure was placed in series with the composite flexure as shown in Figure 2.6.
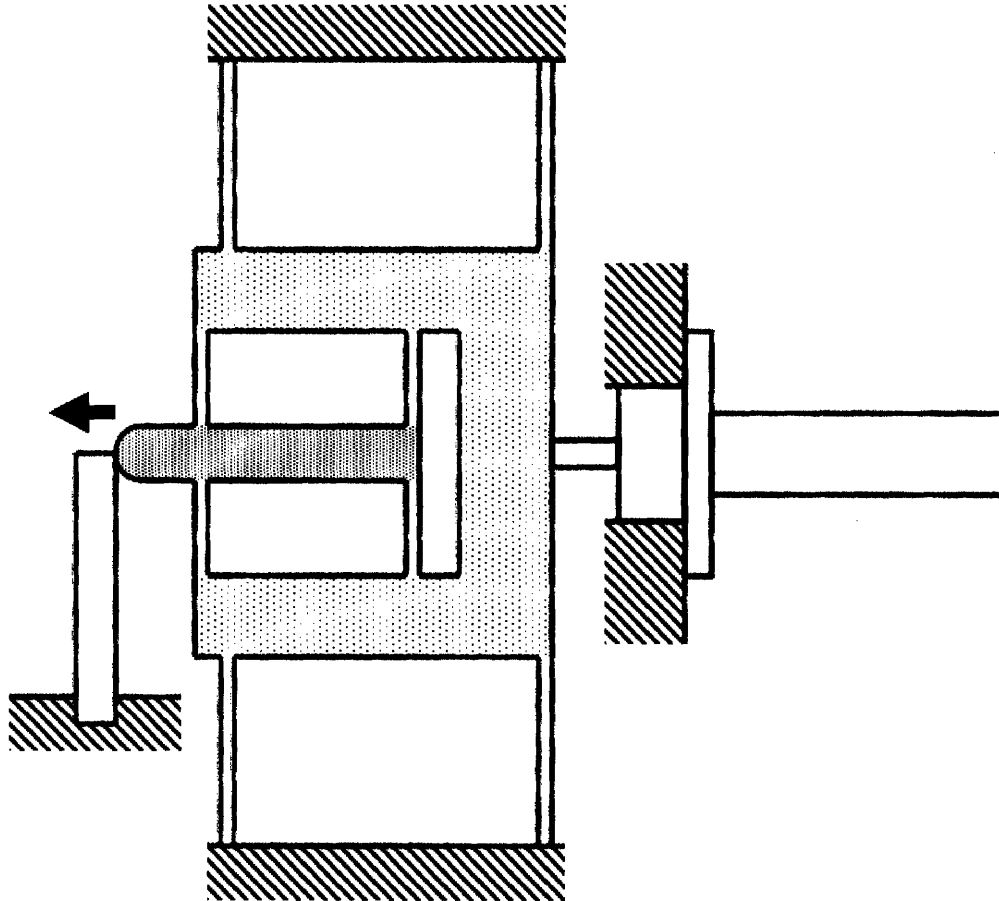
Figure 2.6: Depiction of design 4.

The small flexure would be subjected to the same force felt by the composite flexure. If the stiffness of the small (force measuring) flexure were experimentally obtained by calibrating the system, then a force could be drawn out of the device. In order to avoid weakening the effective degrees of restraint at the tip of the apparatus, the small force flexure was made as a four-bar shuttle. It was placed between the main shuttle body and the tip of the testing apparatus that contacted the composite flexure.

All together, design 4 was able to apply a force without over-constraining the composite flexure, measure displacement and force, and was robust because of its monolithic fabrication. All force and displacement function requirements were met by design 4, so the iterative process was concluded with design 4 as the result.

31

The last part of the design requirements posed at the beginning of this chapter was the need for a suitable anchoring system. This component would not need to move during the test, and only required a way to shift the anchored flexure towards or away from the force-applying tip, so as to bring it into range before the experiment began. The immediate choice for this alignment bearing was a 4-bar compliant shuttle. Using a set screw to position the shuttle, the flexures would apply the needed pre-load to remove any slip in the screw. However, the large size of the alignment shuttle interfered with the force and displacement measuring compliant mechanism unless they were placed horizontally and stacked. In that case, the compliant flexure could be held vertically, and pushed horizontally, as shown in Figure 2.7 below.
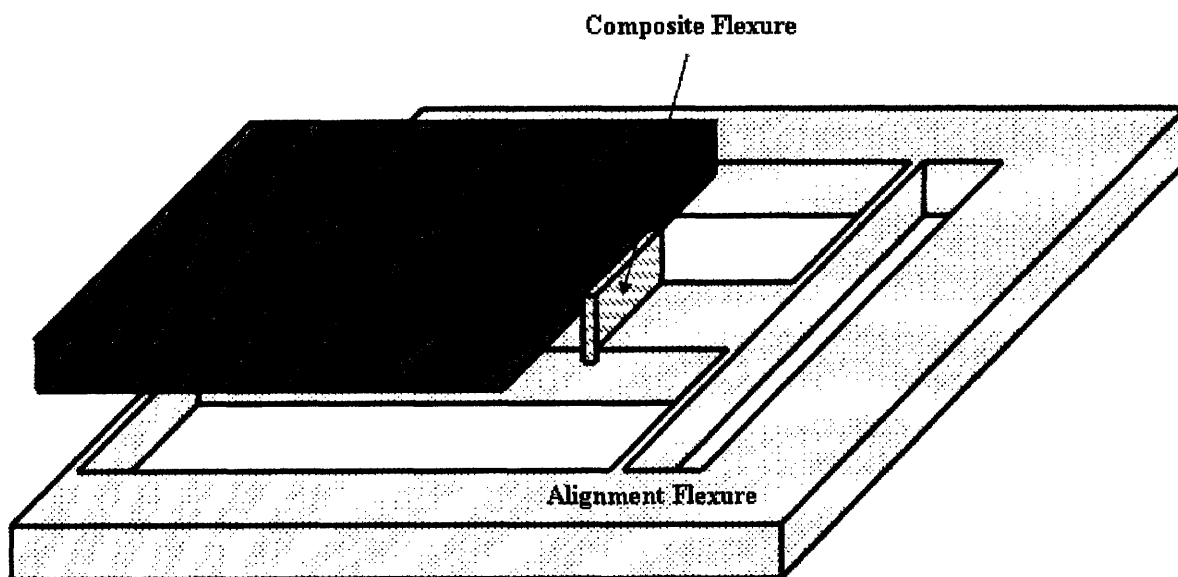
Figure 2.7: Depiction of design 4 with anchoring system.

To hold the flexure, a clamp was favored over glue, owing to the compliance of glue being in series with the composite flexure. This clamp would be placed in the middle of the alignment shuttle, which allows for the composite flexure to be anchored in place, then moved into place by flexing the alignment flexure until it sits directly in front of the force/displacement flexure (labeled Compliant Mechanism in Fig 2.7). The combination of these two devices was sufficient to meet all of the requirements for a testing apparatus, indicating that the design work should continue onto the more detailed phase.

Chapter 3

Modeling of the Design

3.1 Exact Ranges of Requirements

More accurate values for the force and displacement ranges were needed to determine the exact dimensions of the flexures in the testing apparatus. As a first step, the maximum elastic range and force for the composite flexure was calculated using slightly more accurate values. The dimensions of the composite flexure were set at 2 mm height, 0.25 mm thickness and 6.35 mm (¼ inch) width, so as to make it possible for the flexure to be clamped by a part machined from 6.35 mm (¼ inch) thick sheet metal. Also, the 2 mm height would mean that slightly under 1/3 of the 3 mm length tubes would be held in the anchor, and a small fraction of the tubes' length would extend above the point of force application.

Using these dimensions, and a rough approximation of the Young's Modulus ($\approx$3 GPa) for a common epoxy used in CNT composites (SU-8) [5], the transverse stiffness of the flexure was calculated, and then scaled up by a factor of 5 to account for the strengthening of the material from the embedded CNTs. The factor of 5 was an approximation of the largest composite stiffening found in literature [5]. This resulted in a maximum composite flexural stiffness of about 46 kN/m, using the Euler small deflection beam bending equation (Eq. 1.5).

The displacement range of the testing apparatus was determined based on the largest elastic range of the possible flexural materials to be studied. This insured that the range would be sufficient to measure the elastic range for all of the materials that one would wish to test in comparison to the composite flexure. Delrin was found to be the most 'elastic' in this sort. The total range was calculated using the Euler expression for stress as a function of location along the beam, set to the bottom edge of the flexure, as shown in Eq. 3.1,

$$\sigma_{yield} = \frac{y \cdot M(x)}{I}, \tag{3.1}$$

where σ_{yield} is the yield stress of the flexure material, y is the distance from the neutral axis, I is the moment of inertia as described in Eq. 1.4, and $M(x)$ is the moment as a function of distance along the flexure axis. For a simply cantilevered beam of length L with force F applied at the tip, the moment can be described by the expression below.

$$M(x) = F \cdot (x - L) \tag{3.2}$$

Since both the yield stress of the material and its geometry were known, the maximum force, F, was determined, which could then be placed into the Euler beam bending equation (Eq. 1.5 to produce a maximum displacement. To insure that there was sufficient range to determine that the flexure has transitioned into the plastic deformation region, the range was scaled by a factor of two. For Delrin, using commonly available material property values found on the MatWeb on-line materials database [13] (Young's Modulus 3.1 GPa and yield stress 90 MPa), the maximum displacement with safety factor included was calculated to be approximately 617 μm.

The composite flexure stiffness was then multiplied by the total displacement range to give a maximum force of approximately 28.5 N. This value was not scaled in any way because of the factors already used in both the calculation of displacement and flexural stiffness. This value, in conjunction with the composite flexure stiffness and displacement range, was used in the next stage of the design: the calculation of the flexure stiffnesses in the testing apparatus.

3.2 Calculation of Flexure Properties

The qualitative design outlined in the previous chapter was redrawn as a system of springs and masses, so as to calculate the necessary stiffnesses for each of the component flexures. The design was altered slightly upon the realization that the metrology on the testing apparatus (Capacitance -CAP- probes manufactured by Lion Precision) only had a measurement range of 250 μm (assumed to be 200 μm to insure adequate measurement range), less than half of the device range. To solve this, it was eventually determined that a 'reduction' component would be needed, which would be linked to both the main mass and the anchoring mass via flexures. The ratio of these flexures could be adjusted such that at maximum displacement for

the main mass, the reduction mass would have only moved through the range of the metrology system. The resulting model is shown in Figure 3.1 below.
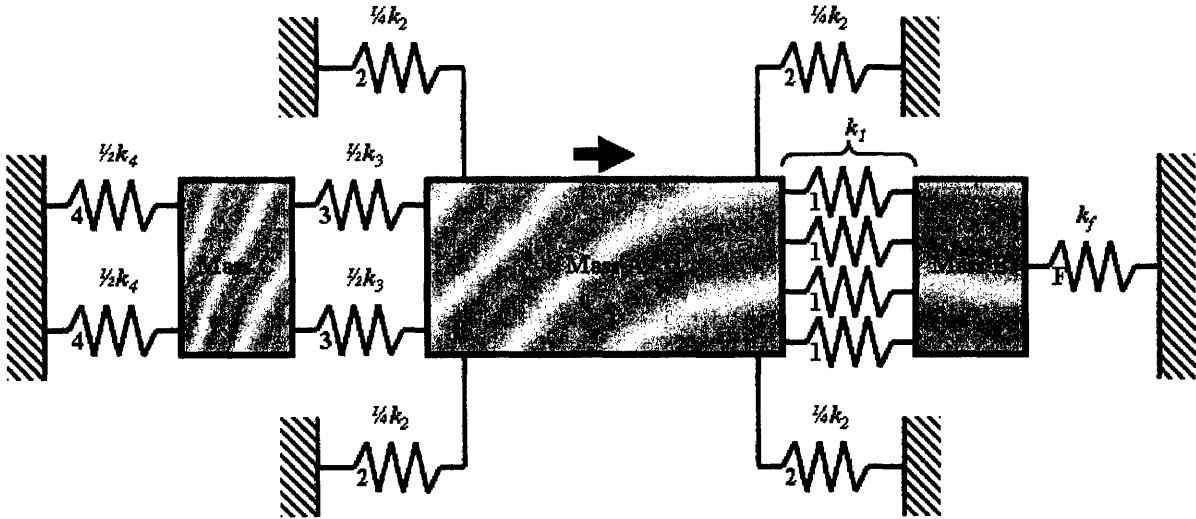

Figure 3.1: Spring-mass model of the compliant testing apparatus.

Mass A is the main shuttle which is driven by the micrometer actuator, while mass B is the force measuring shuttle placed between A and the flexure. Mass C is the reduction shuttle, intended to reduce the movement range of the device back to the range of the metrology system. The composite flexure is modeled as a spring of stiffness k_f, the flexures acting as a linear bearing for the force measuring shuttle are labeled 1, with total stiffness k_1, the flexures acting as a linear bearing for the main shuttle are labeled 2 with total stiffness k_2. The flexures linking the main shuttle to the reduction shuttle are labeled 3 with total stiffness k_3, and finally the flexures resisting the motion of the reduction shuttle are labeled 4 with total stiffness k_4.

The stiffness of the force measuring flexures (1) together was directly calculated as the force range divided by the probe range, to give a value for k_1 of about 143 kN/m.

The ratio of k_4 / k_3 was set as the variable α, which was calculated through simple force balances on B and C resulting in Eq. 3.3 below,

$$\alpha = \frac{\left(\dfrac{k_f + k_1}{k_1}\right)x_f + x_c}{x_c}, \tag{3.3}$$

where x represents the displacement undergone by the composite flexure (f) and the shuttle masses (a,b,c). x_c was set by the 250 μm range of the CAP probes, while x_f was set as the

displacement range of the apparatus. Using these values, α was found to be approximately 3.08, and was used to calculate k_3 once k_4 was known.

This left two undetermined stiffnesses, k_2 and k_4. To set these, the constraint of large natural frequencies was used. The optical table on which the testing apparatus was to be placed effectively damped out high frequency oscillations (>100 Hz), leaving only low frequency vibrations to design around so as not to have the apparatus excite any modes during normal operation. In order to analytically determine the natural frequencies and response to vibrational driving forces, the system was subjected to matrix analysis. The force balance equations for the three masses were written out in the form of Eqs 3.4 below, with the ground, x_D, providing the driving oscillation.

$$\sum F_A = m_A \ddot{x}_A = (x_D - x_A)k_2 + (x_B - x_A)k_1 + (x_C - x_A)k_3$$
$$\sum F_B = m_B \ddot{x}_B = (x_A - x_B)k_1 + (x_D - x_B)k_f \qquad (3.4)$$
$$\sum F_C = m_C \ddot{x}_C = (x_D - x_C)k_4 + (x_A - x_C)k_3$$

The solution was assumed to be an oscillation in the form of Eq. 3.5,

$$x_i = A_i \cos(\omega t) \qquad (3.5)$$

where ω is the driving frequency of the ground, and A_i is the oscillation amplitude of the ith mass. Eq. 3.5 was substituted into Eqs 3.4 and rearranged to form a matrix as shown in Eq. 3.6 below.

$$\begin{bmatrix} -k_2 A_D \\ -k_f A_D \\ -k_4 A_D \end{bmatrix} = \begin{bmatrix} m_A \omega^2 - (k_1 + k_2 + k_3) & k_1 & k_3 \\ k_1 & m_B \omega^2 - (k_1 + k_f) & 0 \\ k_3 & 0 & m_C \omega^2 - (k_3 + k_4) \end{bmatrix} \begin{bmatrix} A_A \\ A_B \\ A_C \end{bmatrix} \qquad (3.6)$$

This matrix was first solved in the absence of driving forces (resetting the left side of the equation to 0) to obtain the un-driven natural frequencies. This was done by setting the determinant of the transfer matrix to 0, and solving for ω. The masses of the shuttles were determined by creating an initial 3D model of the system and measuring the volume of each of the components. Calculations of the upper limit for the mass were carried out given the known density of the aluminum T6-6061 alloy intended for fabrication, resulting in the values: $m_A <$ 0.025 kg, $m_B < 0.005$ kg, $m_C < 0.008$ kg. The values for the mass were iteratively refined throughout the design process and the system natural frequencies were recalculated after each iteration. To obtain a deeper understanding of the dynamics of the system, the expression was

solved for the amplitude responses of the masses A_i, to an oscillatory driving force (assumed to be magnitude 1). Expressions were obtained using Cramer's Rule. These amplitude responses were graphed over a range of frequencies from 10^2 to 10^5 Hz.

Using these two outputs, k_2 and k_4 were adjusted until all of the natural modes occurred at well over 100 Hz, even over 1 kHz. This higher value was set to minimize any gain in the system at 100 Hz or below. Using this method, k_2 was found to optimally be 2 kN/m, while k_4 was found to optimally be 10 kN/m. These values gave the three natural frequencies (corresponding to the three in-plane excitation modes of the 3 shuttle masses) as 1205 Hz, 1389 Hz, and 7329 Hz. The gain as a function of frequency is shown in Figure 3.2 below.
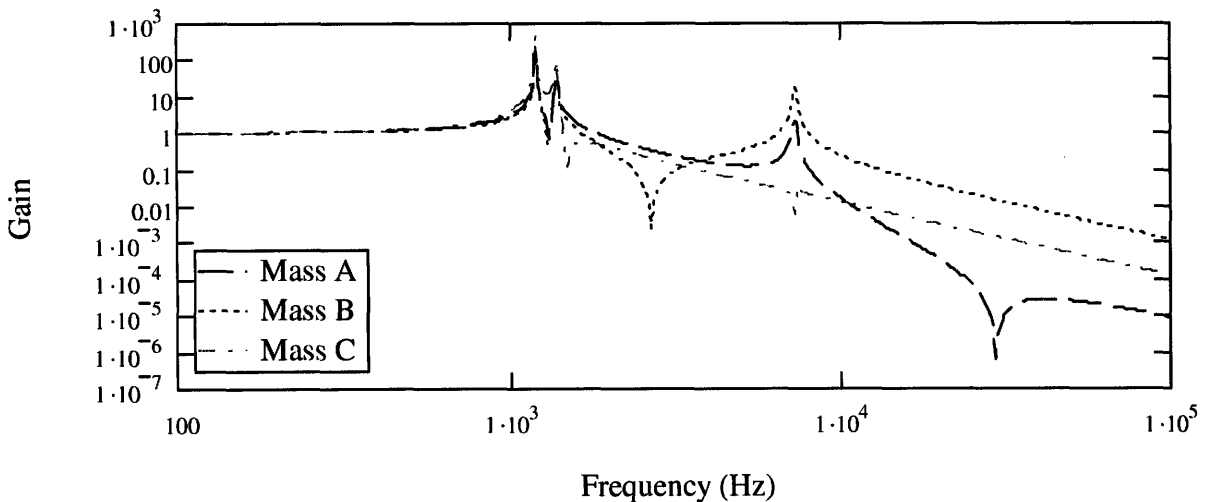

Figure 3.2: Calculated amplitude response of spring-mass model.

The final set of ranges to be determined was the maximum displacement for each of the flexural bearings. The range of the force (1) flexure was already set to the range of the measurement probes (200 μm), as described earlier. For the main shuttle (2) flexures, the range corresponded to the movement required in order to assure that the composite flexure has been displaced to its full range by the force measuring shuttle. In order to calculate this, the force balance on mass B was used as shown in Eq. 3.4, assuming steady state, no driving displacement (x_D =0) and x_B to be the full displacement range (617 μm). This gave the range for the main shuttle flexures to be 817 μm. The anchor to reduction shuttle (4) flexure, as with the force flexure, was set to the range of the measurement probe. This left the reduction shuttle to main shuttle (3) to make up the difference, giving a range of 617 μm. These values are shown in Table 3.1 below.

Table 3.1: Compliant mechanism characteristics

Component	Stiffness (kN/m)	Range (μm)
Composite	46.2	617
Flexure 1	143	200
Flexure 2	2.00	817
Flexure 3	3.24	617
Flexure 4	10.0	200
Mass A	N/A	817
Mass B	N/A	617
Mass C	N/A	200

3.3 Calculation of Flexure Geometry

The ideal geometry for the multiple sets of flexures throughout the testing apparatus was determined to be parallel arrangements of simple rectangular beams, based on the intended use of the flexures as both linear bearings and springs,. The flexures are needed to constrain the shuttle in the two directions while allowing the shuttle to move along one axis. The axial stiffness acts as an excellent equivalent of a constraint because the axial stiffness of the flexure corresponds to normal tension/compression of the beam. The out-of-plane motion is selectively minimized by altering the cross-section of the flexure to be tall and thin, as previously described in section 1.1.

Rectangular flexures have another distinct advantage in that they may be modeled by the Euler-Bernoulli beam bending expression shown in Eq. 1.3, so their geometry may be derived if sufficient information is known about the required elastomechanics. In the case of the flexures in the testing apparatus, the known requirements of maximum range and force made it possible for expressions to be derived for the unknown length L and thickness h. The width b of the flexure is not included here as it is set by the thickness of the sheet metal from which the compliant mechanism is machined. In this case, 6.35 mm (1/4 inch) T6-6061 Aluminum alloy was chosen as the material from which the compliant mechanism would be cut.

For flexures acting as linear bearings, the Euler-Bernoulli beam bending expression takes a slightly different form, since the tip is subject to the condition that it must remain pointing parallel to its non-deformed orientation. This is because both ends of the flexure are anchored to larger pieces of material which do not change angle with respect to one another, as shown in Fig 3.3 below.
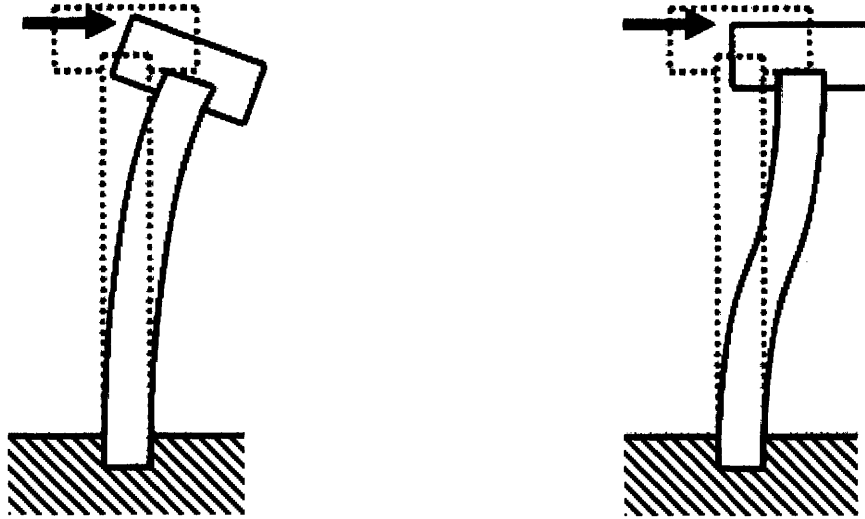

Figure 3.3: End conditions for flexures, unconstrained (a), and parallel tip constraint (b).

In this case, the boundary conditions of 0 slope at each end of the beam for the integration of the Euler-Bernoulli expression give the Eq. 3.7,

$$\delta = \frac{FL^3}{12EI},$$ (3.7)

where δ is the transverse deflection, F is the applied force, E is the Young's modulus and I is the moment of the beam, described by Eq. 1.4. The applied force is directly related to the stiffness of the flexure and its maximum elastic range, removing F as an unknown variable. The second necessary equation for determining the beam geometry is the relation between yield stress σ_y, and applied force, derived from Eq. 3.1 as well as Eq. 1.4 to give Eq. 3.8 below.

$$\sigma_y = \frac{3FL}{bh^2}$$ (3.8)

The two equations 3.7 and 3.8 provide sufficient information to determine the two unknowns, L and h. By combining these two equations, the necessary length L of the beam can be set as Eq. 3.9 below,

40

$$L = \frac{3\delta E^{2/3} k^{1/3}}{b^{1/3} \frac{\sigma_y}{S}},$$ (3.8)

where S is an arbitrary safety factor, to insure that at maximum displacement, the flexures are still operating within the elastic range. This value was set at a large value, 5, for the calculations as any plastic deformation would quickly destroy the calibration for the device. Through the same process, the necessary thickness h of the beam can be set as Eq. 3.10.

$$h = \frac{3\delta E^{1/3} k^{2/3}}{b^{2/3} \frac{\sigma_y}{S}}$$ (3.8)

Using these two equations, and the commonly available material property values for 6061 Aluminum found on the MatWeb on-line materials database [14] (Young's Modulus 70 GPa and yield stress 240 MPa), the necessary flexural geometries were calculated as shown in Table 3.2. The exact dimensions of the compliant mechanism can be found in Appendix A.

Table 3.2: Flexural geometries

Component	Length (cm)	Thickness (mm)
Flexure 1	3.77	1.63
Flexure 2	3.72	0.386
Flexure 3	4.15	0.639
Flexure 4	1.96	0.439

3.4 System Structure Design

The flexural system described in the previous section was designed to be a monolithic compliant mechanism, acting as a mechanical transfer function; the input is a driving displacement and the output is two other displacements which correspond to the force and deflection experienced by the sample under study. In order to link the inputs and outputs to useful structures, the compliant mechanism was integrated into a larger mechanical system, able to provide the needed displacements, and read the distance readings produced by the mechanism. A micrometer was placed in-plane with the compliant mechanism, centered on the symmetric axis of the device so as to produce displacement only in the axial direction, as shown in Fig. 3.3 below.
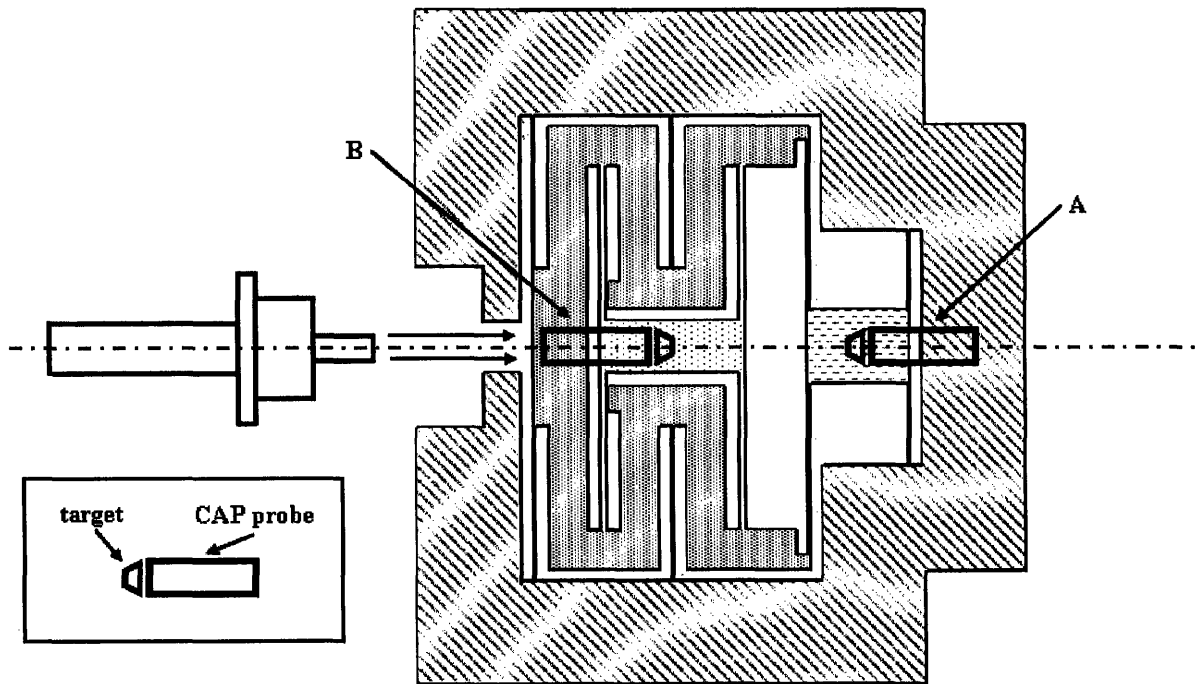
Figure 3.3: Schematic illustration of sensing and actuating components.

Two CAP probes were used to monitor the shuttle locations on the compliant mechanism, one reading the motion of the reduction shuttle (A) corresponding to displacement measurements and the other reading the motion of the force shuttle relative to the main shuttle (B). This was then set on stands which would be anchored to an optical table. Finally, a second alignment flexure was designed to sit on top of the main compliant mechanism, and hold the composite flexure in place, as shown in Fig. 2.7. The alignment flexure was designed as a linear bearing with range larger than the sum of the machining errors, so that any mis-match in the alignment could be compensated for at the beginning of the experiment. The flexure was driven by a set screw to bring the composite flexure into contact with the testing apparatus, so that the experiment could be carried out within the range of the device.

Chapter 4

Physical Implementation

4.1 Fabrication and Assembly

The parts of the testing apparatus were waterjetted from sheets of T6-6061 Aluminum, then machined to achiever errors of roughly 50 μm (0.002 in) in part dimensions. The parts were then assembled on an air-damped optical table and surrounded in a removable environmental control chamber, as shown in Fig. 4.1 below so as to reduce thermal variation as well as minimize ambient noise vibration. Lion Precision capacitance (CAP) probes were used to measure the displacement of components, and the probe outputs were read at 100 Hz by the D-Space Matlab interface program. A graphical interface was written to read out both the raw probe data, and the moving 200-pt average.
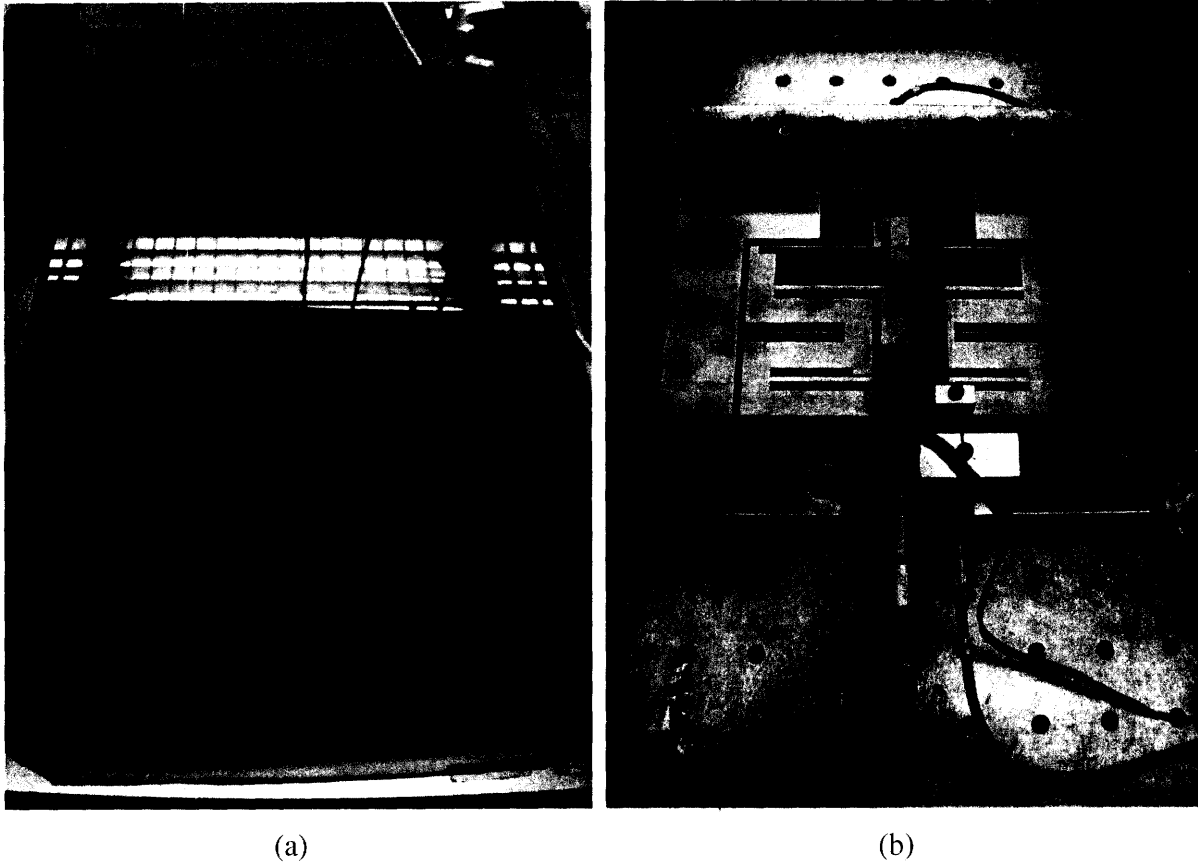
(a)   (b)

Figure 4.1: Physical setup of assembly (a) with top removed for detail (b).

4.2 Force Calibration

4.2.1 Experimental Setup

The exact stiffness of the flexural bearings for the force shuttle was measured in order to determine the force applied to the composite flexure. The displacement readings from the measurement probes could then be translated into a force value through Hooke's Law, assuming the bearings showed a linear response. If the bearing showed significantly non-linear behavior, then a fit function would be set to the calibration data, and this fit would be used to translate the displacement into a force. The system was re-assembled vertically so that weights of measured mass could be hung directly below the flexure, applying a constant and known force so as to collect the necessary force and displacement data on the 'force' flexures,. The new orientation of the whole compliant mechanism in the vertical direction made it possible for weights to be used to produce a force directly in parallel with the degree of freedom for the flexures. The

arrangement shown in Fig. 4.2 below was used to align the weights direction below the center of the force shuttle.
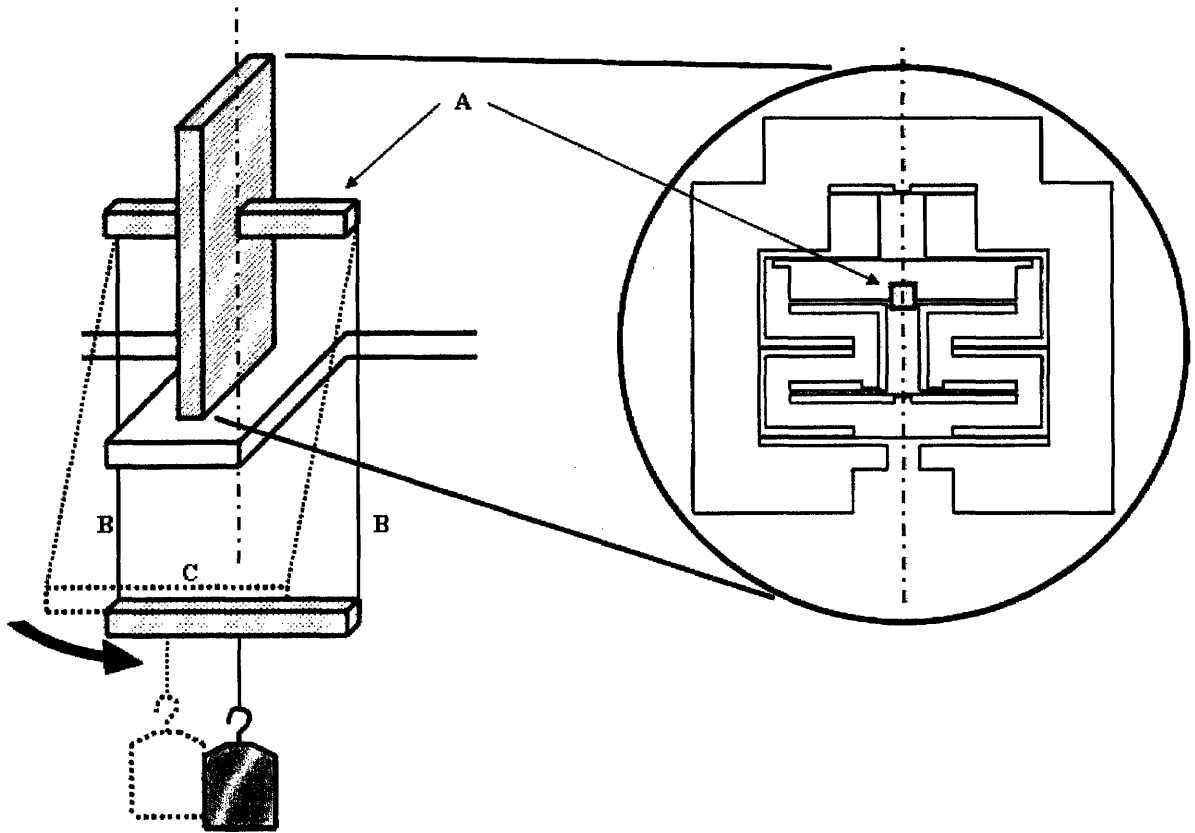

Figure 4.2: Illustration of force calibration setup.

A beam (A) was placed on the tip of the force shuttle, orthogonal to the plane of the compliant mechanism. Symmetric anchoring points were used on (A) on either side of the plane of the compliant mechanism, to which strings (B) of equal length were hung. Each of the strings was then attached to one end of a second beam (C) oriented parallel to A, and having the same dimensions. This created a four bar mechanism composed of two parallel beams (A, C) and two parallel strings (B), which was theoretically free to shift in two horizontal degrees of freedom as shown until the weights hung from the middle of beam C lined up exactly below the center of force for the shuttle linear bearing. In practice, the waterjetted beams were of close enough dimensions that with suitable adjustment to the lengths of the strings, the system acted as desired.

4.2.2 Calibration Results

As described, weights of various mass were hung from the midpoint of beam C to produce the desired force. These weights were measured by a standard tabletop digital scale with an accuracy of 1 gram, while the displacement was measured by a CAP probe running at 100 Hz, and time averaged over 200 points to give an accuracy of 20 nm. The resulting data and fit are shown below, in Fig. 4.3.
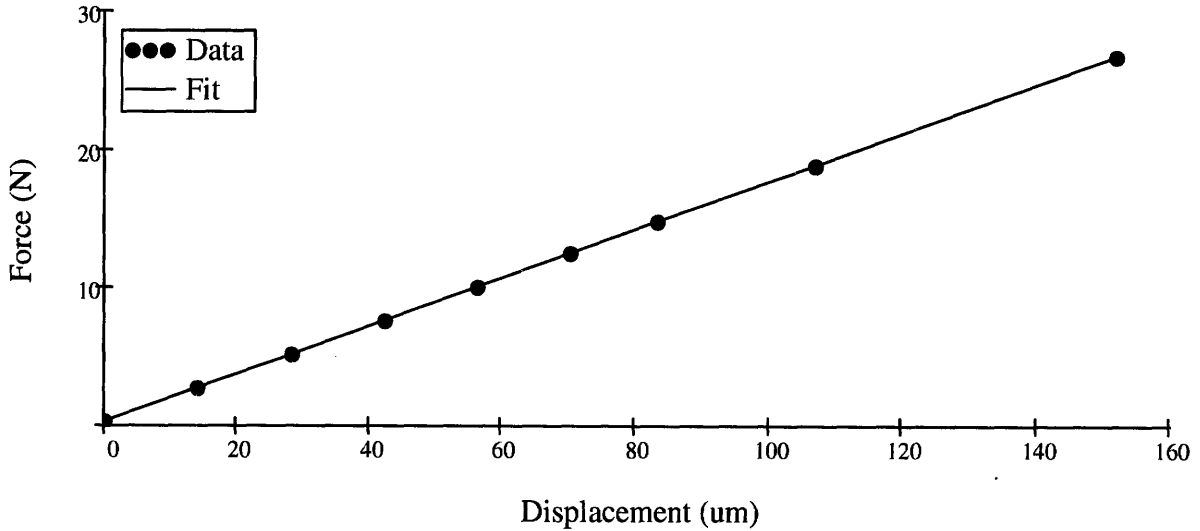

Figure 4.3: Force calibration curve.

As can be seen in Fig. 4.3, the resulting fit was best approximated by a line, conforming to the assumption of linearity in the flexure's elastomechanics. The linearity of the curve means that only the slope of the line (k_{calc}) is necessary for calibration, which was found to be 0.1751 N/µm. Once the experiment is begun, the only required calculation for force F is found by subtracting off the initial value of the CAP probe x_{B0} from the present reading x_B and multiplying this resulting distance by the calculated stiffness k_{calc}, as shown in Eq. 4.1 below.

$$F = k_{calc}(x_B - x_{B0}) \qquad (4.1)$$

To calculate error for the system, the measurements for selected points through the range were redone, resulting in a known repeatability of measurement of about 100 nm, corresponding to a force measurement repeatability of 0.018 N. When the average error of the fit-line was calculated, it resulted in almost the same value (0.021 N), indicating that the dominant error of the system in the force transfer function is accounted for by the repeatability of the CAP probes.

Additionally, the error was not found to be proportional to the displacement but rather was a constant value throughout the full range. This corroborated the hypothesis of CAP probe repeatability as the dominant error source, for the probe's observed distribution around a given value would result an equivalent and uniform distribution of force values precisely as observed in the calibration.

4.3 Displacement Calibration

4.3.1 Experimental Setup

To determine the exact displacement occurring at the force-applying tip of the testing apparatus, the device was run over its full range while the position of both the main shuttle and reduction shuttle was measured with CAP probes. As with the force calibration, two results were possible. If the relation was linear, then the displacement could be calculated in a form similar to Eq. 4.1, however if the relation was non-linear then a high-order curve could be fit to the data points. An additional mounting point was attached to the device to collect the needed values for this calibration. This new mounting point made it possible for a calibrating probe to be placed adjacent and parallel to the micrometer, as shown in Figure 4.4.
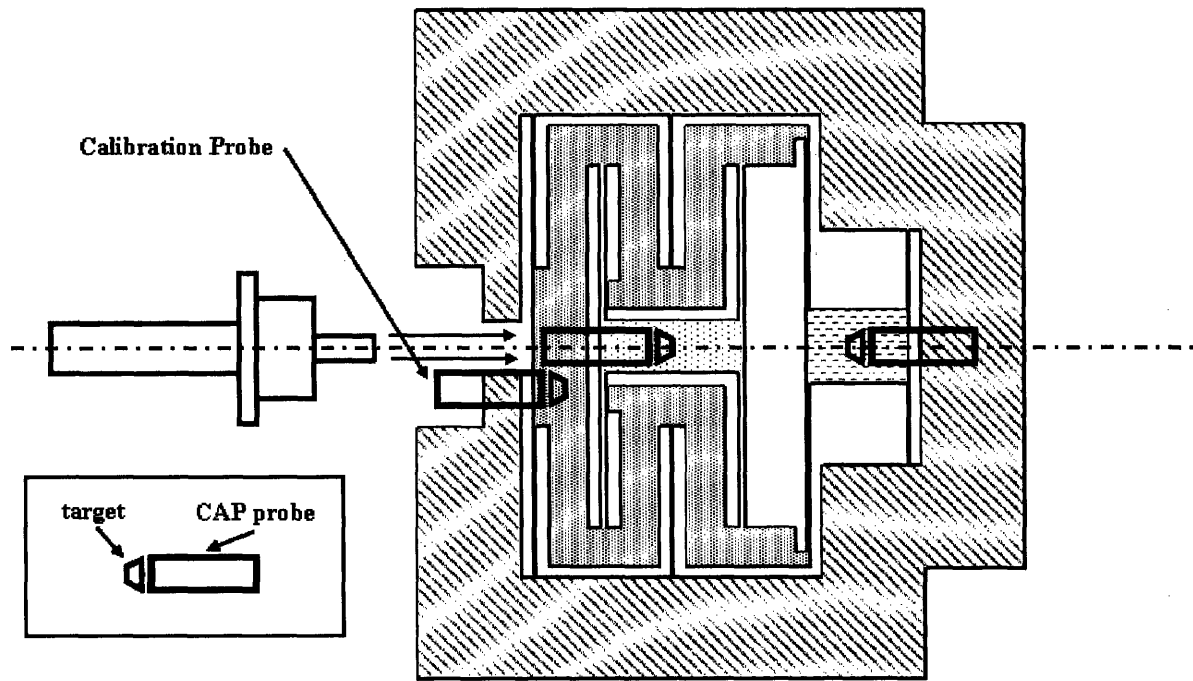

Figure 4.4: Displacement calibration experimental setup.

The calibration probe allowed for a direct measure of the displacement of the main shuttle near the symmetric axis (see Fig 3.3), which reduced the measurement error associated with the internal flexing of the main shuttle.

4.3.2 Calibration Results

The results from the two probes were graphed as shown in Fig 4.5 with a 5th order polynomial expression was fit to the data. This fit followed from the assumption that the curve passes through the origin. The calibration probe was physically reset every 230 microns to the close end of its range in order to measure over the 800 micron range of the main shuttle,. During this resetting process, the rest of the system was held steady, so as to link the 'before' and 'after' values of the calibration probe to both correspond to the same physical state of the system.
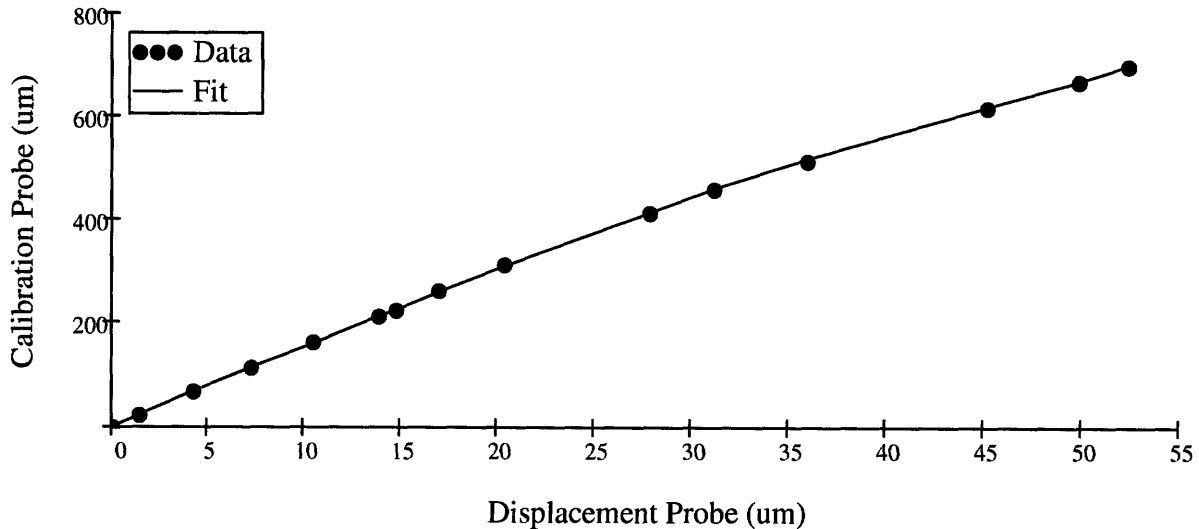

Figure 4.5: Displacement calibration curve.

The system was designed for all of the flexures to operate well within their elastic range, only running up to 1/5 of the yield point at maximum deflection. Based on this, it was assumed that the ratio of stiffnesses between flexures 3 and 4 would remain a constant throughout the range. However, as is apparent in Fig. 4.3, the curve is linear at first, then begins to flatten off, indicating that the ratio of flexures changes as the displacement of both increases. In particular, the reduction in slope corresponds to a reduction in the stiffness of k_4 relative to k_3. Since k_3 is about 1/3 of the stiffness of k_4, it deflects 3 times as far for a given force. It appears that at the approximately 300 micron displacement at which the non-linearity begins, the weaker set of flexures (3) are actually being deformed far enough that strain stiffening occurs. This is an

increase in the transverse stiffness of the flexure due to axial stretching of the flexure, which is caused by the constraint that the tip must remain the same vertical distance from the base of the flexure- a common problem with flexural linear bearings under moderate deformation.

The no-load zero point for the flexural system must be found before each experimental run because of the non-linearity. As with the force calibration, the initial CAP probe reading x_{A0} is subtracted off from the present reading x_A, and this normalized distance is fed into the fit function $f_{fit}(x)$ to calculate the displacement of the main shuttle. The force shuttle is able to move relative to the main shuttle during the test, so the full displacement calculation requires this distance $x_B - x_{B0}$ be subtracted from the main shuttle displacement, as shown in Eq. 4.2 below, where δ is the displacement experienced by the composite flexure.

$$\delta = f_{fit}(x_A - x_{A0}) - (x_B - x_{B0}) \tag{4.2}$$

As with the force calibration, the error of the system was characterized by the average difference between the fit line and the measured data points, which was found to be 1.2 μm. This is the result of the same situation as observed in the force calibration, where the repeatability of the probes at around 100 nm. The coefficients for the fit, as shown in Table 4.1 below, indicate that the first order term is the dominant one for the majority of the range. This results in a first order calculation of error of about 1.5 μm, only slightly higher than what was observed. As with the force calibration, the close correspondence between observed and predicted error indicates that the error in the displacement measurements can be completely characterized by the repeatability of the CAP probes.

Table 4.1: Displacement calibration coefficients

1st Order	1.519 x 10^1
2nd Order	1.423 x 10^{-2}
3rd Order	5.976 x 10^{-4}
4th Order	-8.267 x 10^{-5}
5th Order	1.012 x 10^{-6}

4.4 Parasitic Motion

During the calibration, it was noticed that actuation of the compliant testing mechanism with the micrometer caused a slight displacement to occur in the force flexure, even though the

force shuttle was not in contact with any object. This parasitic force reading is believed to be due to the compression of the main shuttle as force is applied to it. The main shuttle has a C shaped design, with each end of the C ending in accordion-like folding. This was intended to make the design more compact, and any flexing was minimized by making the width of the potentially flexible parts about 1 order of magnitude larger than the width of the flexural members. The cubic relation between stiffness and width means that there should be a roughly three orders of magnitude difference between the shuttle internal flexing and the linear bearings constraining it. With the linear bearings moving on the order of 1 mm, the shuttle would then be compressed by about 1 μm, pulling the force shuttle back by roughly that amount, as shown in Fig. 4.6 below.
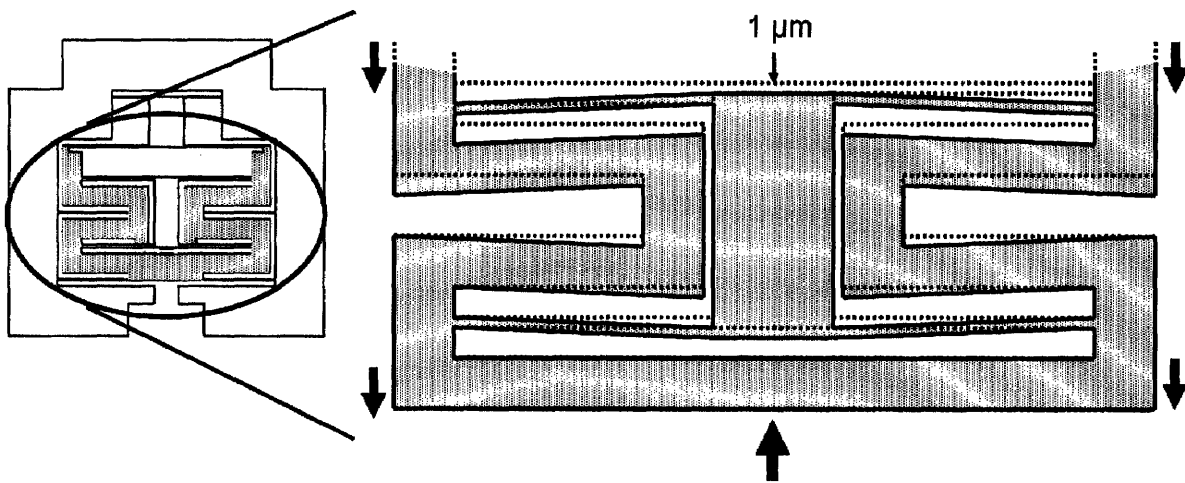

Figure 4.6: Displacement calibration curve.

The amount of parasitic motion was observed to be in this range of 1 μm, which would produce an error in the force measurement of up to 0.18 N, significantly more than the error due to the probe repeatability. The force shuttle displacements were collected during the general displacement calibration and compared to the main shuttle displacement, as shown in Fig. 4.7 below.
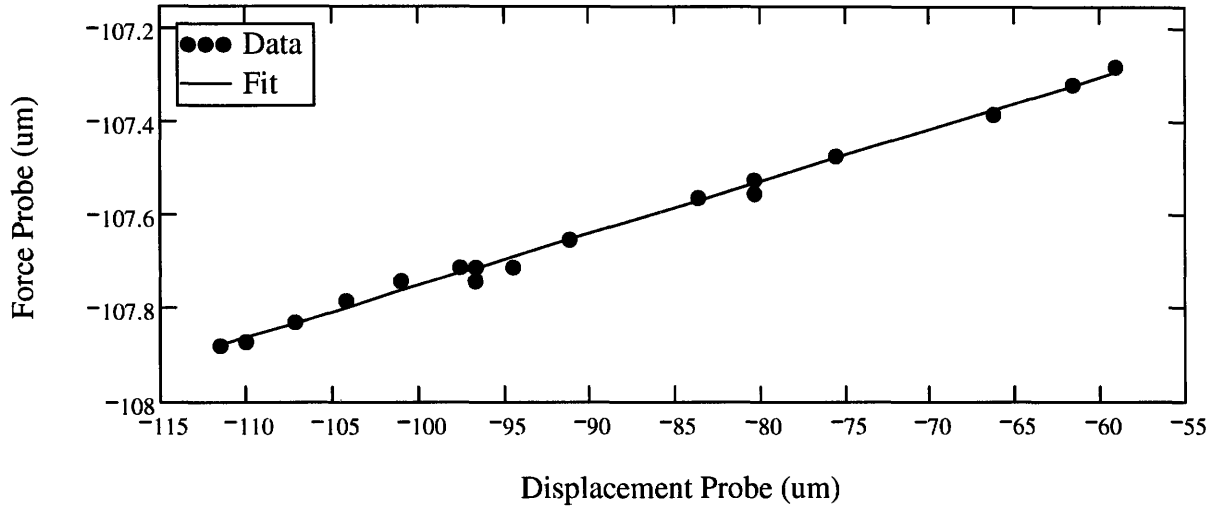
Figure 4.7: Parasitic motion calibration curve

The relation between these two displacements was clearly linear, resulting in a characterization of the parasitic motion simply by a translational constant (corresponding to the slope of the line) C_T of 0.0112. This new effect altered the calculation for the force (Eq. 4.2), leading to the new expression shown in Eq. 4.3 below.

$$F = k_{calc}(x_B - x_{B0}) - k_{calc}C_T(x_A - x_{A0})$$ (4.1)

Chapter 5

Conclusion

The objective of this research is to explore the feasibility of using aligned-CNT composites as flexural members in compliant mechanisms. Compliant mechanisms rely on flexures to produce motion of components within the device. These flexures enable very precise and repeatable motion which can be deterministically linked to the force applied to the flexure. CNTs are relatively strong, nanometer scale tubes of graphene that have the potential to vastly increase the mechanical properties of composites in the same way that carbon fibers are used on the micro-scale to strengthen composites. It is believed that CNTs may be able to increase both the stiffness and elastic range of the matrix material in which they are embedded because of their extraordinarily high Young's modulus and yield strength,. Flexures made of this composite would be able to function over a larger range. With larger ranges, compliant mechanisms could be reduced in scale and integrated into new devices such as SEMs or other microscopy equipment.

5.1 Summary

The work presented in this thesis is the first stage in the process of evaluating CNT-based composites. In order to test the composites, a suitable testing apparatus must be obtained or developed. Using this apparatus, composites can be tested for their mechanical properties. The optimal composite may then be reached through iterative cycles of fabrication and testing. The results of the work are outlined below:

- A functional design for a testing apparatus that represents the most effective candidate for obtaining data.
- The fabrication of a physical apparatus.

- Characterization of the apparatus's performance, including error measurement and the calculation of the transfer function between experimental output and applied force/displacement.

A set of system requirements was drawn up and compared to existing designs for both macro- and nano-scale testing machines in the attempt to find a pre-existing machine capable of carrying out the testing. The meso-scale nature of the requirements placed these machines at the far limits of usability, indicating that an apparatus would need to be custom designed to the task. A series of designs were considered, culminating in the adoption of a compliant mechanism design capable of measuring both applied force and displacement through relative motion of sub-components. This design was then modeled in order to optimize its performance within the designed force and displacement ranges. The result of this analysis was a set of dimensions corresponding to the geometries of the flexures in the compliant mechanism. A testing mechanism was designed using these dimensions which, in conjunction with anchoring stands for probes and actuators were integrated into a full testing system.

The testing apparatus was fabricated from sheet metal T6-6061 Aluminum using CNC water-jet cutting to achieve the needed accuracy and CNC milling to produce the flat interface surfaces. It was set up in an environmental control cover so as to minimize thermal and mechanical transients. A control interface was written to display the probe readings for recording purposes.

The testing apparatus was calibrated with regards to both its force and displacement measurements, by applying known values and comparing with the probe readouts. Fit curves were calculated, which were used to determine the force/displacement experienced by the composite flexures during testing. The error in both of the measurements were calculated using the analysis of the fit curves. A possible mechanism was proposed for explaining the error, and was compared favorably with several observations.

5.2 Future Work

Given the two phase nature of this project, the remaining work can be easily split into two general categories, that of alterations to the testing apparatus, and that of fabrication of composites.

5.2.1 Alterations to the Testing Apparatus

It was initially desired that the testing apparatus would be driven by a linear actuator, so as to enable rapid data collection and even cyclic testing. This was not accomplished due to time constraints. The addition of a motorized actuator would remove the manual element of the testing, potentially automating the entire testing process. This would bring several benefits. First, rapid creep was observed on some materials, so being able to quickly capture the data would give a more accurate characterization of the material. Secondly, one of the large concerns in flexure materials design is minimizing the hysteresis of the flexure. This problem could be accurately quantified by repeated cyclic testing of the composite flexures using a linear actuator.

It would be quite useful to be able to image the actual micro-scale physical processes occurring in the composite flexure as it deforms. Unfortunately, it is presently only possible to image the composite after the experiment is complete. Imaging makes it possible to characterize the damage incurred through deformation. If the testing apparatus could be miniaturized slightly, it could possibly be mounted in an SEM, making it possible to image the CNT composite micro-scale response to strain in real-time. A simpler but less useful method for real-time observation would be to mount the testing apparatus under an optical microscope. However, these composites are generally uniformly black, and thus show little detail when observed in visible light.

5.2.2 Fabrication of Composites

As of writing this thesis, preliminary results have been obtained on composite flexures. A significant amount of work has been done towards producing an aligned-CNT composite, however, the full description of the theory and process is far beyond the scope of this thesis. As a simple overview, the fabrication of composites will require several steps. Aligned CNT forests of roughly 3 millimeter height must be grown or obtained from other laboratories, as was done for this thesis. There are as yet no commercial channels for such material. Methods must be developed for wetting these forests without producing air pockets. These methods will be similar to work that has already been done on wetting smaller scale CNT forests of about 50 μm [10]. The composite must then be shaped into the flattened rectangular geometry required by the testing apparatus. The shaping can be done either by significant post machining of a large piece of composite or by growing the CNT forests to compress under wetting to the desired geometry.

Finally, several experimental methods for compressing the CNT forests to produce higher density should be studied, as this will likely produce better mechanical properties for the composite. Work has progressed to the point of producing wetted CNT forests, post-machined to the required flexural geometries. These composite flexures will be compared to purely epoxy-based composites of the same size to study the effects of adding CNTs. Pure epoxy flexures have been fabricated and tested, as shown in Fig 5.1.
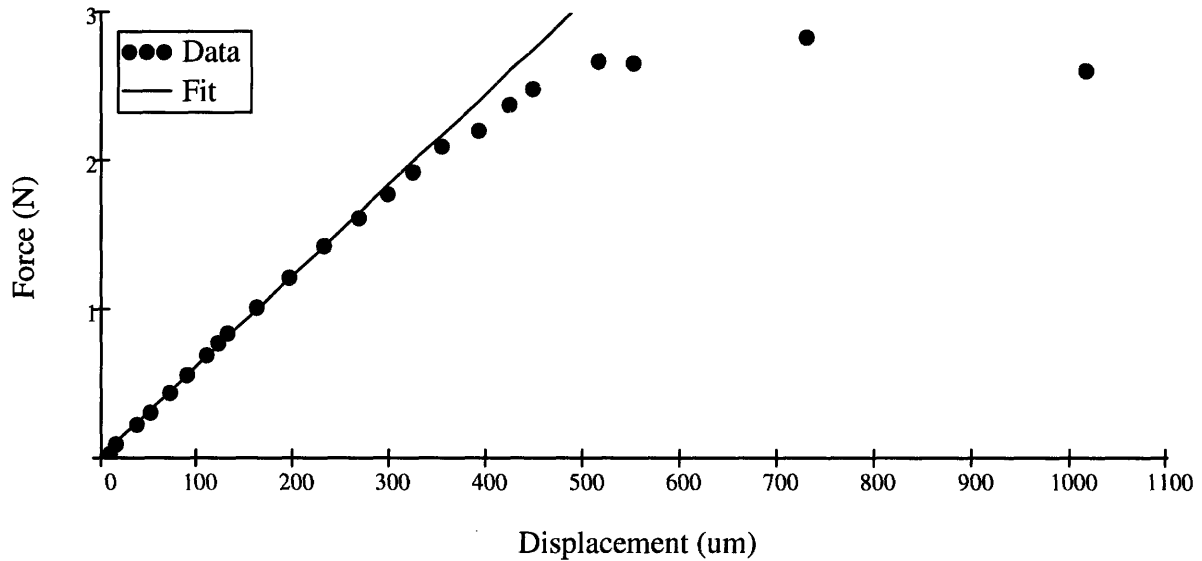

Figure 5.1: Experimental results of pure EpoThin flexure

A slope was fit to the linear (elastic) region of the flexure as shown with the blue line, and using this as the effective stiffness of the flexure, a Young's modulus of 0.63 GPa and yield stress of 26 MPa were derived for the material using Eq. 1.5, 3.1 and 3.2. The exact values for these properties are unknown, but they appear to be in the range common to most polymers.

References

[1]   L.L. Howell. Compliant Mechanisms Wiley Interscience (2001).

[2]   M. Meyyappan Ed. Carbon Nanotubes: Science and Applications. CRC Press LLC (2005).

[3]   S. Iijima. Nature **354** (6348), 56 (1991).

[4]   L.X. Zheng, Proceedings from the NSTI Nanotechnology. Conference & Trade Show (2005).

[5]   Jonathan N. Coleman, Umar Khan, Werner J. Blau and Yurii K. Gun'ko. Carbon **44** (9), 1624 (2006).

[6]   Xiaojing Xu and Kin Liao, Material Physics and Mechanics **4** 148 (2001).

[7]   Jeroen W. G. Wilder, Liesbeth C. Venema, Andrew G. Rinzler, Richard E. Smalley, Cees Dekker. Nature **391**, 59 (1998).

[8]   Boris I. Yakobson, and Phaedon Avouris. Topics in Applied Physics **80**, 287 (2001).

[9]   Hideki Mori, Yoshihiko Hirai, Shigenobu Ogata, Seiji Akita and Yoshikazu Nakayama, Japanese Journal of Applied Physics **44** (42), 1307 (2005).

[10]   E. J. Garcia, A. J. Hart, B. L. Wardle, A. H. Slocum. "Fabrication of Composite Microstructures by Capillarity-Driven Wetting of Aligned Carbon Nanotubes with Polymers", Submitted to Nanotechnology (2007).

[11]   Zwick/Roell. "Allround-Line Product Info." <http://www.zwick.co.uk/docs/Allround-Table1.pdf>. Accessed April 4, 2007.

[12]   Hysitron, Inc. "TriboIndenter, 3D OmniProbe Upgrade." <http://www.hysitron.com/ PDF/OP-01.pdf>. Accessed April 4, 2007.

[13]   Automation Creations, Inc. "Dupont Delrin® Acetal, homopolymer, unfilled, extruded." <http://www.matweb.com/search/SpecificMaterial.asp?bassnum= P1SM03> Accessed Oct. 15, 2006.

[14]   Automation Creations, Inc. "Alclad Aluminum 6061-T6, T651" <http://www. matweb.com/search/SpecificMaterial.asp?bassnum=MA6061AT6> Accessed Oct. 15, 2006.

Appendix A: Compliant Mechanism

Appendix A describes the exact dimensions of the Compliant mechanism composing the testing apparatus. The holes in this component are used to anchor the rest of the testing system to the various shuttles in the compliant mechanism.
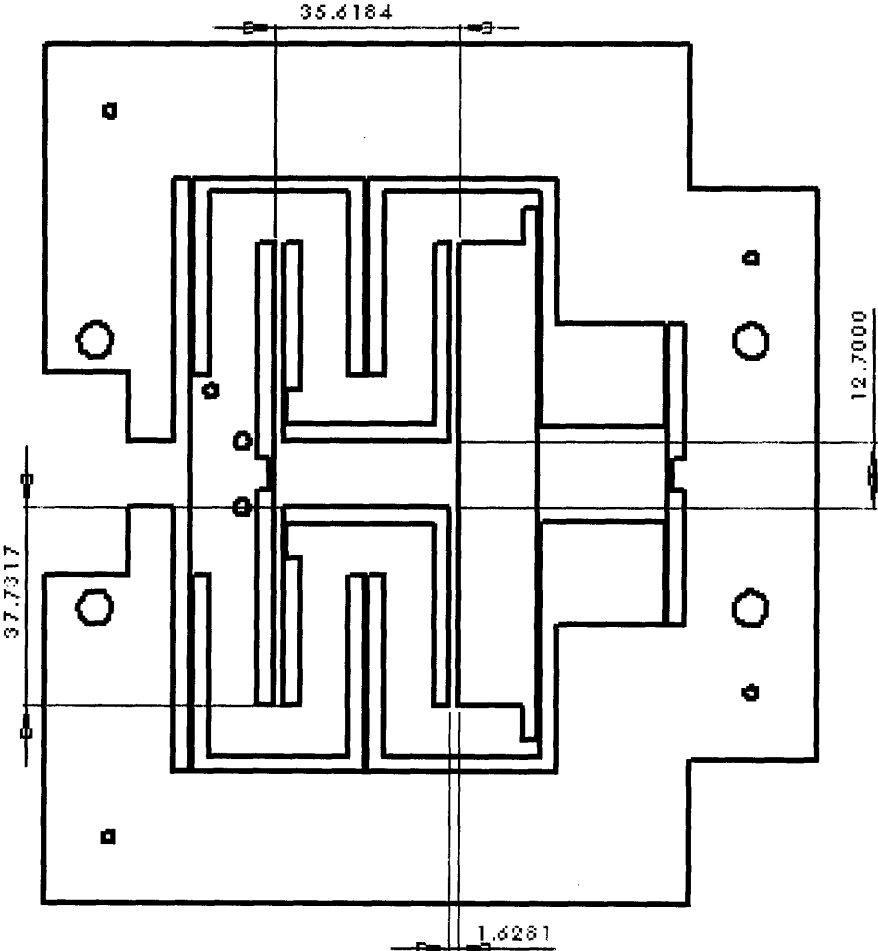

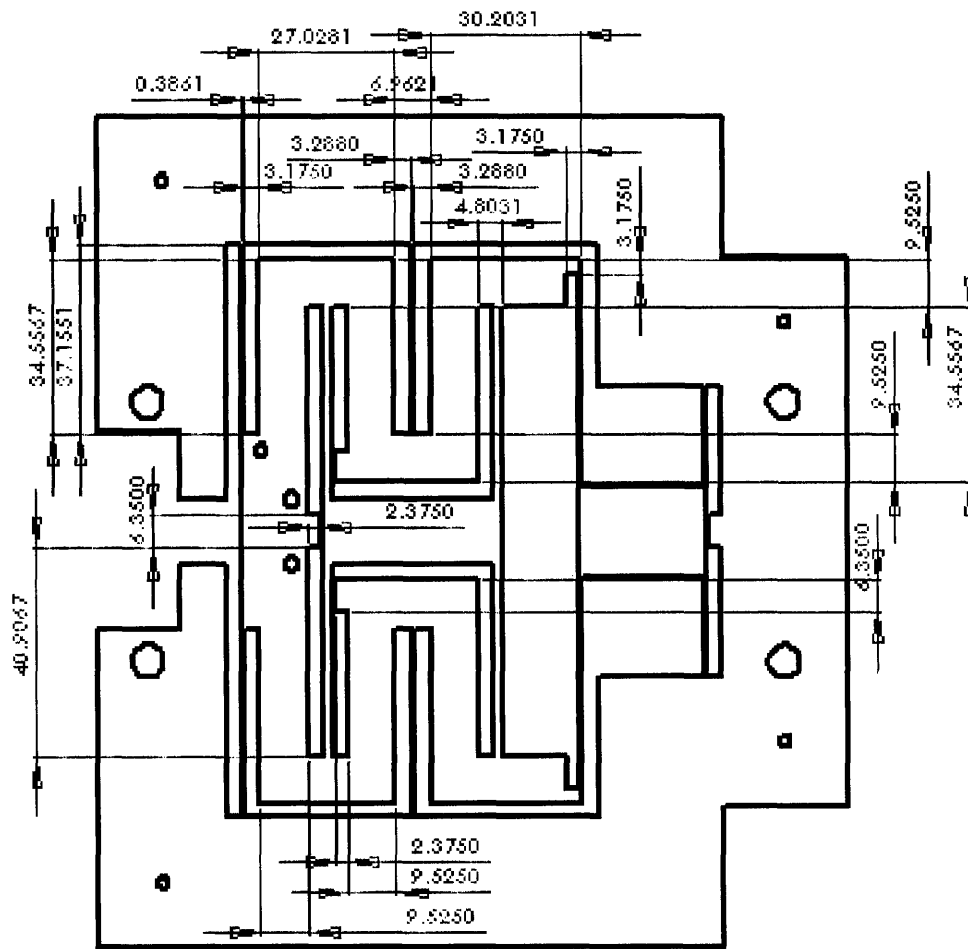*Figure A1: Dimensions of force shuttle and (1) flexures in mm*

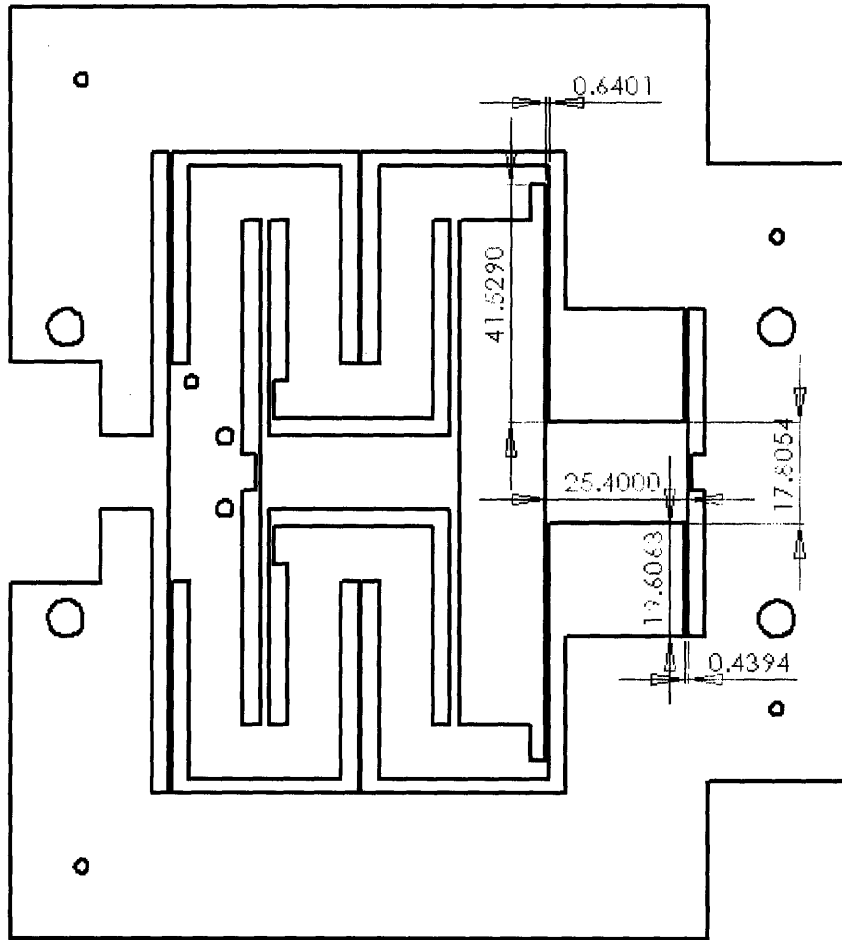*Figure A2: Dimensions of main shuttle and (2) flexures in mm*
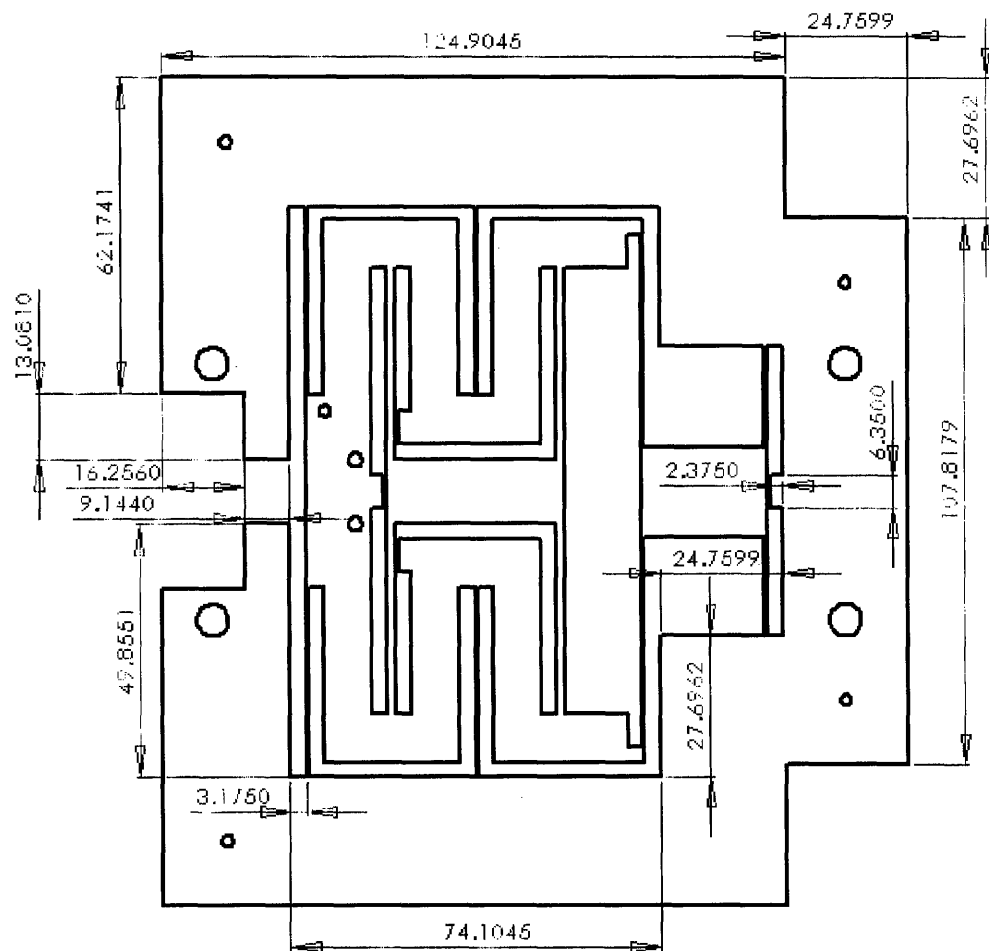
60

Figure A3: Dimensions of displacement shuttle, (3) and (4) flexures in mm

Figure A4: Dimensions of base in mm